2022年2月 February, 2022
矿 床 地 质 MINERAL DEPOSITS
第41卷 第1期 41 (1): 69~90

文章编号: 0258-7106 (2022) 01-0069-22
Doi: 10. 16111/j. 0258-7106. 2022. 01. 005

长江中下游成矿带龙角山矽卡岩钨矿床成矿作用过程
——来自白钨矿和石榴子石主微量元素的证据*

聂利青[1,2],周涛发[2**],蔡国军[1],孙孝峰[3],宋玉龙[3],蔡 毅[1],殷 帅[1],王凤云[1]

(1 安徽建筑大学土木工程学院智能地下探测技术重点试验室,安徽 合肥 230601; 2 合肥工业大学资源与环境工程学院,安徽 合肥 230009;3 湖北省地质局第一地质大队,湖北 大冶 435000)

摘 要 白钨矿和石榴子石的原位微量元素特征能提供成矿流体的演化信息。长江中下游成矿带鄂东南矿集区龙角山矿床是近年发现的大型矽卡岩钨矿床,为区域找矿勘查和成科学研究提供了新的方向。龙角山矿床的流体演化和矿床成因亟待开展系统研究。文章在详细的野外工作和前人研究基础上,通过对矿床中矽卡岩阶段、退蚀变阶段和石英硫化物阶段的白钨矿和石榴子石进行原位主、微量分析,厘定了矿床成矿过程的环境和矿质沉淀机制。龙角山矿床矽卡岩阶段的红棕色石榴子石(Grt-1)矽卡岩、黄绿色石榴子石(Grt-2)-辉石矽卡岩和脉状石榴子石(Grt-3)-硅灰石矽卡岩中石榴子石成分分别为 $Adr_{30.6\text{-}84.1}Gro_{13.9\text{-}50.7}Pyr_{1.5\text{-}30.3}$、$Adr_{38.3\text{-}100}Gro_{0.0\text{-}39.4}Pyr_{0.0\text{-}22.4}$ 和 $Adr_{75.3\text{-}100.0}Gro_{0.0\text{-}13.9}Pyr_{0.0\text{-}12.7}$,且富集大离子亲石元素,亏损高场强元素,具有富集轻稀土元素、亏损重稀土元素、铕正异常的特征。龙角山矿床矽卡岩阶段石榴子石 U 含量逐渐降低,且与钙铁榴石的成分变化吻合,表明在矽卡岩阶段成矿流体氧逸度逐渐升高;退蚀变阶段到石英-硫化物阶段白钨矿 Mo 元素含量先升高后降低,对应的氧逸度先增加后降低,显示了成矿过程复杂的脉冲式的氧逸度变化特征。龙角山矿床退蚀变阶段和石英-硫化物阶段的白钨矿显示铕负异常减弱、正异常增加的变化特征,表明成矿流体的 pH 值逐渐增加,而非在退蚀变阶段(主成矿阶段)达到峰值。因此,pH 值不是影响白钨矿沉淀的主要因素。龙角山矿床矽卡岩阶段 Grt-1 稀土元素总量与 Y 存在正相关关系,Grt-2 和 Grt-3 稀土元素总量与 Y 无正相关关系,且 Grt-3 富 Fe 元素,表明随着石榴子石的结晶由热液平衡状态向非平衡条件转变,水岩反应程度逐渐增加;退蚀变阶段(主成矿阶段)Sch-1 的不规则生长环带比石英硫化物阶段 Sch-2 更发育,表明主成矿阶段水岩反应程度达到峰值,水岩反应是控制该矿床矿质沉淀的重要因素。流体混合和水岩反应是控制龙角山矿床钨沉淀的主要机制,二者协同控制白钨矿沉淀成矿,龙角山矿区具有成大矿、富矿的潜质。

关键词 地质学;白钨矿;石榴子石;微量元素;成矿作用;龙角山矿床
中图分类号:P618.67 **文献标志码**:A

Mineralization process in Longjiaoshan skarn tungsten deposit of Middle-Lower Yangtze River Metallogenic Belt: Constraints from in situ major and trace element analysis of garnet and scheelite

NIE LiQing[1,2], ZHOU TaoFa[2], CAI GuoJun[1], SUN XiaoFeng[3], SONG YuLong[3], CAI Yi[1], YIN Shuai[1] and WANG FengYun[1]

(1 Key Laboratory of Intelligent Underground Detection Technology, School of Civil Engineering, Anhui Jianzhu University, Hefei 230601, Anhui, China; 2 School of Resource and Environmental Engineering, Hefei University of Technology, Hefei 230009, Anhui, China; 3 No.1 Geological Party of Hubei Geological Bureau, Daye 435000, Hubei, China)

---

* 本文得到安徽省教育厅高校科学研究项目(编号:KJ2021ZD0069)和国家自然科学基金项目(编号:91962218)联合资助
第一作者简介 聂利青,女,1993 年生,博士,讲师,矿物学、岩石学、矿床学专业。Email:nielq@mail.hfut.edu.cn
** 通讯作者 周涛发,男,1964 年生,教授,博导,矿物学、岩石学、矿床学专业。Email:tfzhou@hfut.edu.cn
收稿日期 2021-08-29;改回日期 2022-01-04。秦思婷编辑。

Abstract

In situ trace element characteristics of scheelite and garnet provide the evolution information of ore-forming fluids. The Longjiaoshan deposit is a large skarn tungsten deposit discovered in southeastern Edong orefield of the Middle-Lower Yangtze River Metallogenic Belt (MLYB). The fluid evolution history of the deposit has not been systematically studied, which restricts the prospecting work and theoretical research of the MLYB. Based on detailed field work and previous studies, this study carried out in situ major and trace elements analyses of scheelite and garnet formed at different stages. The composition of red-brown garnet (Grt-1), yellow-green garnet (Grt-2)-pyroxene skarn and veined wollastonite-garnet (Grt-3) from the Longjiaoshan deposit is $Adr_{30.6\text{-}84.1}Gro1_{3.9\text{-}50.7}Pyr_{1.5\text{-}30.3}$, $Adr_{38.3\text{-}100}Gro_{0.0\text{-}39.4}Pyr0_{.0\text{-}22.4}$ and $Adr_{75.3\text{-}100.0}Gro_{0.0\text{-}13.9}Pyr_{0.0\text{-}12.7}$, respectively. These three types of garnet are rich in LILEs and LREE, depleted in HFSEs and show positive Eu anomaly. The content of U element in garnet from the Longjiaoshan deposit gradually decreases, which is consistent with the composition change of andradite, indicating that the oxygen fugacity of ore-forming fluid gradually increases in the skarn stage. From retrograde to quartz-sulfide stage the Mo content of scheelite increases and then decreases, as well as the oxygen fugacity increases and then decreases, indicating the complex pulse oxygen fugacity change characteristics in the mineralization process. The scheelite formed in the retrograde alteration stage and quartz sulfide stage shows decreasing in Eu negative anomaly but increasing in Eu positive anomaly, indicating that the pH value of ore-forming fluids gradually increases. Therefore, pH value is not the main factor affecting scheelite precipitation. In the Skarn stage, there is a positive correlation between the total REE and Y of Grt-1, but there is no positive correlation between the total REE and Y of Grt-2 and Grt-3, and Grt-3 is rich in Fe, indicating that the degree of water-rock reaction increases gradually as the crystallization of garnet changes from fluid equilibrium state to non-equilibrium condition. Moreover, the irregular growth zones of Sch-1 in the retrograde stage (main mineralization stage) is more developed than Sch-2 in the quartz sulfide stage, indicating that the water-rock reaction degree reaches the peak in the main mineralization stage, that is, the water-rock reaction is an important factor controlling the ore mineral precipitation. Fluid mixing and water-rock reaction are the main mechanisms controlling tungsten precipitation in the Longjiaoshan deposit. The Longjiaoshan area is a prospective terrane for the formation of large and high grade W ore deposits.

Key words: geology, skarn, scheelite, garnet, trace elements, mineralization, Longjiaoshan deposit

白钨矿和石榴子石作为矽卡岩型矿床中普遍存在的金属矿物和硅酸盐矿物(Meinert et al., 2005；Goldmann et al., 2013；Poulin et al., 2016；Guo et al., 2016；Xiong et al., 2017；Sciuba et al., 2019；Liu et al., 2020；Zhang et al., 2020)，随着矿物原位分析(in-situ analyses)的不断进步和激光剥蚀电感耦合等离子质谱仪(LA-ICP-MS)技术的推广(Crowe et al., 2001；周涛发等, 2010；Reich et al., 2013；Huang et al., 2015；汪方跃等, 2017)，白钨矿和石榴子石的原位微量元素特征被广泛应用于解释成矿流体物理化学条件和组分，进而反映成矿流体演化和水岩反应程度(Ghaderi et al., 1999；Brugger et al., 2000；Song et al., 2014；Sun et al., 2017；Zhao et al., 2018；Li et al., 2018；Zhang et al., 2018；Harlaux et al., 2018；Wu et al., 2019；Han et al., 2020)。除岩相学特征外，阴极发光(CL)也是揭示矿物环带特征的强有力技术手段，并且已经成功应用于多种矿物(例如石英、磷灰石、碳酸盐矿物；McManuset al., 1992；Campbell et al., 1997；Gotze et al., 2002；Redmond et al., 2004；Rusk et al., 2008；Müller et al., 2010；Poulin et al., 2016)，并用于指示成矿作用。特别是CL图像直接与激光原位面扫描图像和微量元素结合阐述矿物复杂的振荡环带，记录矽卡岩成矿系统中脉石矿物和矿石矿物结晶时热液流体的组成、性质和演化(Cottrant, 1981；Gaft et al., 1999；Brugger et al., 2000；Mair, 2006；Roberts et al., 2006；MacRae et al., 2009；Zhaiet al., 2014；Poulin et al., 2016)，并反演热液矿床中流体特征和为成矿动力学背景提供重要信息(Sverjensky, 1984；Giere, 1996；Uspensky et al., 1998；Ghaderi et al., 1999；Brugger et al., 2000；Hazarika et al., 2016;Qi et al., 2020;Su et al., 2021)。

长江中下游成矿带是中国矿床学研究的热点地区之一(周涛发等,2012),也是“层控矽卡岩矿床”(常印佛等,1991)和“斑岩-矽卡岩复合成矿理论”(翟裕生等,1992)的发祥地。近年来在长江中下游成矿带新发现的钨矿床为该成矿带的研究提出了新的课题(周涛发等,2019)。龙角山矿床是成矿带鄂东南矿集区内新发现的大型矽卡岩型钨多金属矿床。鄂东南矿集区从南东到北西,矿化类型呈钨—钨铜—铜铁—铜—铁扇形过渡,是研究长江中下游成矿带钨与铜、铁成矿作用关系的理想对象。前人对龙角山矿床的研究主要集中于成岩成矿年代和岩体地球化学特征(丁丽雪等,2014)、稳定同位素和流体包裹体(Lei et al., 2018)以及矿物电子探针主量元素分析(纪云昊等,2019)等方面,但矿床成矿作用的环境和矿质沉淀机制的研究则相对薄弱。本文在矿床地质特征和前人研究工作基础上,对龙角山矿床的白钨矿和石榴子石开展了系统的矿物学和原位微区地球化学特征研究,试图厘定该矿床的成矿流体演化特征,分析钨的沉淀机制,提高成矿带钨矿床成矿作用的研究程度并为找矿勘探提供理论依据。

1　矿床地质特征

1.1　区域地质背景

长江中下游成矿带内金属矿床(点)达200余处,主要集中在八大矿集区(常印佛等,1991;周涛发等,2017;图1a、b),成矿带内的矿床主要有4种类

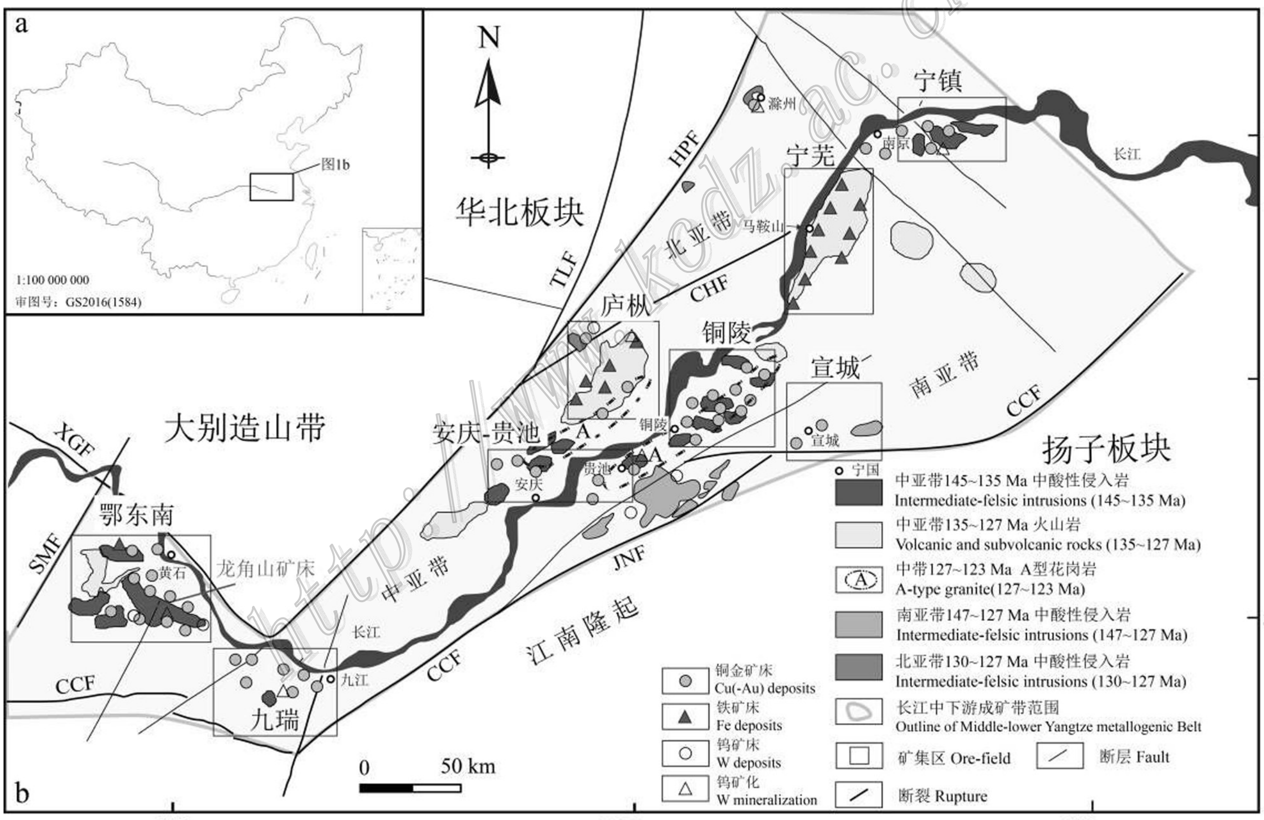

http://www.kcdz.ac.cn/

图1　长中下游成矿带矿床分布示意图(据常印佛等,1991;周涛发等,2017)

a. 中国地质略图;b. 长江中下游成矿带地质图

XGF—襄樊-广济断裂;TLF—郯庐断裂;HPF—黄-破断裂;SMF—商麻断裂;CCF—崇阳-常州断裂;CHF—滁河断裂;JNF—江南断裂

Fig. 1　Geologic map of magmatic rocks and deposits in the Middle-Lower Yangtze River Metallogenic Belt (MLYB) (after Chang et al., 1991; Zhou et al., 2017)

a. Geology sketch of China; b. Geologic map of MLYB

XGF—Xiangfan-Guangji rupture; TLF—Tancheng-Lujiang rupture; HPF—Huang-Po rupture; SMF—ShangMa rupture; CCF—Chongyang-Changzhou rupture; CHF—ChuHe rupture; JNF—JiangNan rupture

型:① 矽卡岩-斑岩型铜-金-钨矿床,其成矿作用与143~140 Ma的花岗闪长岩类侵入岩体关系密切,主要分布在铜陵矿集区、鄂东南矿集区、九瑞矿集区、安庆-贵池矿集区和宣城矿集区(Mao et al., 2006;Xie et al., 2007;王世伟等,2012;谢桂青等,2013;徐晓春等,2014;Xiao et al., 2021);② 矽卡岩型钨钼矿床,其成矿作用与135 Ma的花岗闪长岩类侵入体关系密切,主要分布在皖南地区(宋国学等,2010;丁宁,2012);③ 玢岩型铁(钨)矿床(化)(磁铁矿-磷灰石型矿床),成矿作用与130 Ma左右的辉长闪长玢岩关系密切,主要分布在宁芜矿集区、庐枞矿集区和鄂东南矿集区(张乐骏等,2011;范裕等,2011;Xie et al., 2015;Nie et al., 2017);④ 与酸性岩相关的金(铀)-钨矿床,成矿时代为108~97 Ma,主要分布在宁镇矿集区和庐枞矿集区(孙洋等,2014;聂利青等,2016a;张赞赞等,2018;Zhang et al., 2021)。前人对上述4类矿床开展了系统的研究工作,建立了多层楼矽卡岩模式(常印佛等,1991)、玢岩铁矿模式(宁芜玢岩铁矿编写组,1978)等,并指出燕山期的陆内俯冲是造成长江中下游成矿带大规模成岩和成矿作用的主导机制(Lü et al., 2015;2021)。近年来,一系列钨矿床(化)在长江中下游成矿带内被相继发现(周涛发等,2019),"南钨北扩"界限逐步向北扩展,钨矿床可独立产出,也可与成矿带内各类金属矿化共、伴生,成矿时代跨度大,成矿类型均为矽卡岩型(宋国学等,2014;颜代蓉等,2012;聂利青等,2016b;2018;陈雪锋等,2017),如湖北省大冶市铜山口铜矿床、安徽省庐江县龙桥铁矿床、安徽省铜陵市姚家岭锌金矿床均发现共、伴生钨矿化(朱乔乔等,2014;张维,2017;钟国雄等,2014)。

鄂东南矿集区发育有著名的"大冶式"大型富铁矽卡岩型铁矿床(如铁山、程潮、金山店)、斑岩-矽卡岩复合型铜钼矿床(铜山口和丰山洞)、矽卡岩型铜金矿床(鸡冠嘴和鸡笼山)、矽卡岩型铜钨矿床(龙角山阮家湾)和中国最大的矽卡岩型铜铁矿床(铜绿山),这些矿床均属于与燕山期中酸性侵入岩有关的成矿系列(谢桂青等,2008)。根据地球化学元素分布特点,鄂东南矿集区分为4个成矿地球化学区,呈扇形展布,即鄂城-金山店-灵乡亲铁元素地球化学区、黄石-大冶亲铁元素和亲铜元素地球化学区、阳新亲铜元素地球化学区、殷祖-丰山亲铜元素和钨钼族元素地球化学区(舒全安等,1992)。

1.2 矿床地质特征

龙角山钨矿床位于鄂东矿集区阳新岩体西侧(图2),是鄂东南矿集区内新发现的大型钨矿床。龙角山矿区于1956~1972年进行补充勘探和深部地质找矿工作,2006年、2010~2012年湖北省鄂东南地质大队对龙角山矿区的港沟山矿段和港背山矿段进行铜钼钨矿普查地质工作,2018~2019年湖北省鄂东南地质大队对龙角山矿区进行外围找矿工作,现已探明矿床钨资源量5.84万吨,铜资源5.5万吨(湖北省第一地质大队,2018),目前该矿床钨资源量已达到大型规模,进一步的勘探工作正在进行,有望扩大资源量。

龙角山矿区内地层主要为志留系中统坟头组、石炭系中统黄龙组和大埔组、二叠系下统栖霞组和茅口组、二叠系上统龙潭组、下窑组和大隆组、三叠系下统大冶组。地层整体呈北东东向,倾向北北西。矿区出露岩体有花岗闪长斑岩、闪长玢岩、煌斑岩,钻孔揭露成矿岩体为花岗闪长斑岩(图3),该岩体成岩年龄为(144±1)Ma,成矿作用发生于(144.7±2.9)Ma(丁丽雪等,2014)。矿体主要赋存在付家山向斜的北西翼和港沟山背斜的南东翼。

龙角山钨矿床中钨矿体产于花岗闪长斑岩与和二叠系下统茅口组(图4a)、栖霞组(图4b)接触带,由多个不连续的透镜状矿体组成;钨钼矿体产于花岗闪长斑岩与二叠系下统栖霞组、茅口组接触带(图4a),矿体总体走向北东,倾向南西,矿体沿走向和倾向延伸数百米。金属矿物主要为白钨矿、辉钼矿、黄铁矿,少量黄铜矿、磁铁矿、方铅矿、闪锌矿;非金属矿物主要为钙铝榴石、钙铁榴石、透辉石、硅灰石、阳起石、绿帘石、绿泥石、磷灰石、方解石、硬石膏和石英等矿物。

根据矿物的结构构造和共生组合,可以将龙角山矿床的热液期分为矽卡岩阶段、退蚀变阶段、石英-硫化物阶段和碳酸盐阶段(图5)。矽卡岩阶段矿物组合为石榴子石-辉石-硅灰石,由岩体向大理岩延伸,矽卡岩种类依次为红棕色石榴子石内矽卡岩(图6a、d)、黄绿色石榴子石-透辉石外矽卡岩(图6b、e)、脉状石榴子石-硅灰石外矽卡岩(图6c、f)。退蚀变阶段矿物组合为白钨矿、阳起石、绿帘石、绿泥石、磷灰石、磁铁矿,白钨矿交代先形成的石榴子石等矽卡岩矿物(图6g),呈团块状包裹在石榴子石粒间或环带(图6h、i)。石英-硫化物阶段矿物组合为石英、黄铜矿、黄铁矿、白钨矿(图6j、k)、辉钼矿、方铅矿、闪锌矿、磁黄铁矿、硬石膏,白钨矿呈半自形与黄铁矿等硫化物共生(图6l)。碳酸盐阶段矿物组合为方解石、白云石、石英等矿物。

http://www.kcdz.ac.cn

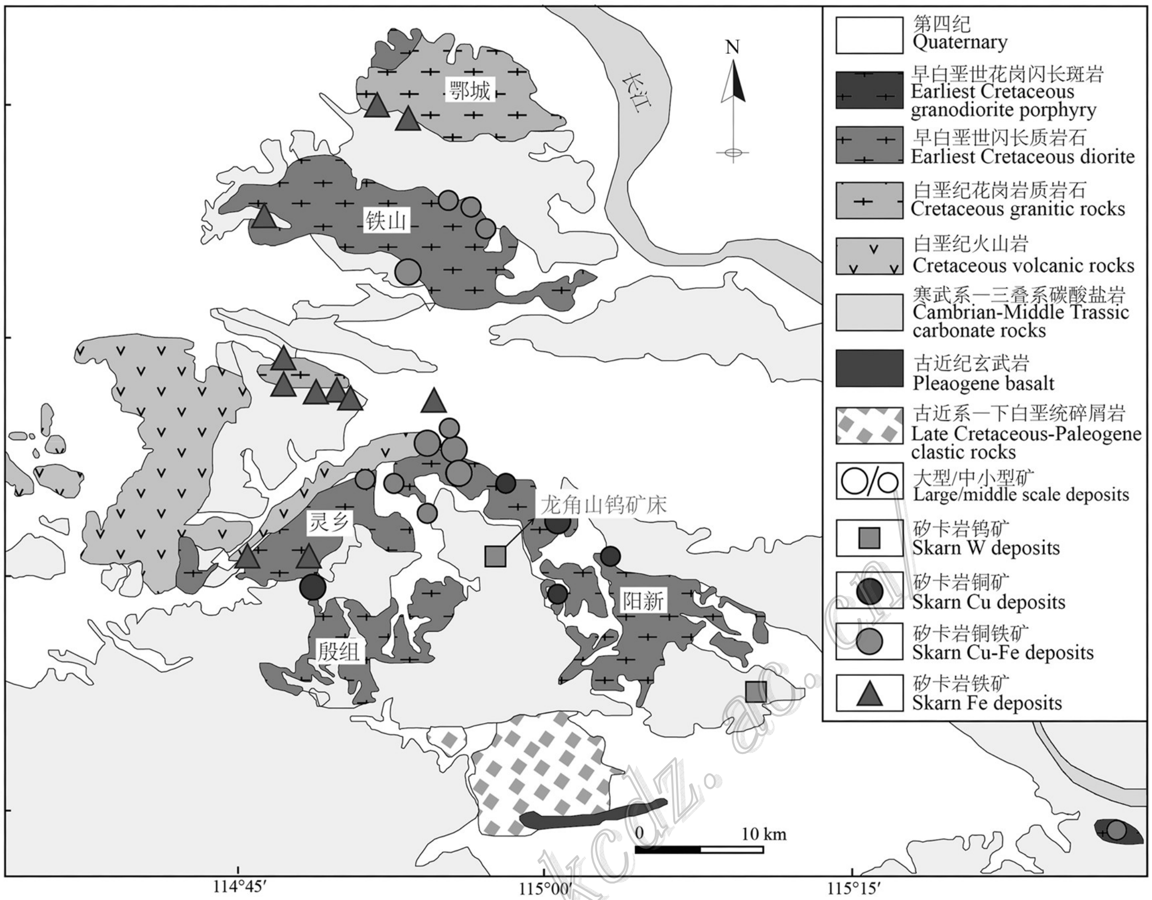

图2 鄂东南矿集区地质简图(据谢桂青等,2008修改)

Fig. 2 Geological sketch map of the Edong orefield (modified after Xie et al., 2008)

http://www.kcdz.ac.cn

1.3 采样特征

本次所测石榴子石和白钨矿样品分别采自龙角山矿床的不同钻孔(图4a、b)。

红棕色石榴子石内矽卡岩样品号为5402-551、5403-487、6601-878、6602-681,黄绿色石榴子石-辉石外矽卡岩样品号为5401-607、5402-456、5403-339、6601-705、6602-569,脉状石榴子石-硅灰石外矽卡岩样号分别为5403-283、6602-531;退蚀变阶段白钨矿样品号为5403-377、5403-398、6601-780、6602-603;石英-硫化物阶段白钨矿样品号为5401-645、5402-491、5403-417、5403-450,其中,样号前4位为钻孔号,后3位为钻孔取样深度。

2 测试分析方法

样品微观形貌分析在合肥工业大学资源与环境工程学院矿床成因与勘查技术研究中心(OEDC)矿物微区分析实验室热场发射扫描电镜Tescan MIRA3(设备配置布鲁克60mm2 EDX能谱仪,阴极发光仪)上完成。

主量元素电子探针(EPMA)分析在合肥工业大学资源与环境工程学院完成仪器型号为JEOL JXA 8230。实验条件为:加速电压15 kV,束斑尺寸3 μm,探针电流20 nA。所有元素的信号采集时间均为15 s,背景时间均为5 s,修正方法ZAF,检测限优于100×10^{-6}。

微量元素和面扫描激光剥蚀电感耦合等离子质谱(LA-ICP MS)分析在合肥工业大学矿物原位分析实验室完成。电感耦合等离子体质谱仪由美国安捷伦公司制造,型号为Agilent 7900。激光剥蚀系统为莱伯泰科公司制造的Analyte HE。ArF准分子激光发生器产生193 nm深紫外光束,经匀化光路聚焦于矿物表面。激光束斑直径为30 μm,频率为8 Hz,剥蚀时间40 s,以高纯He气为载气,与

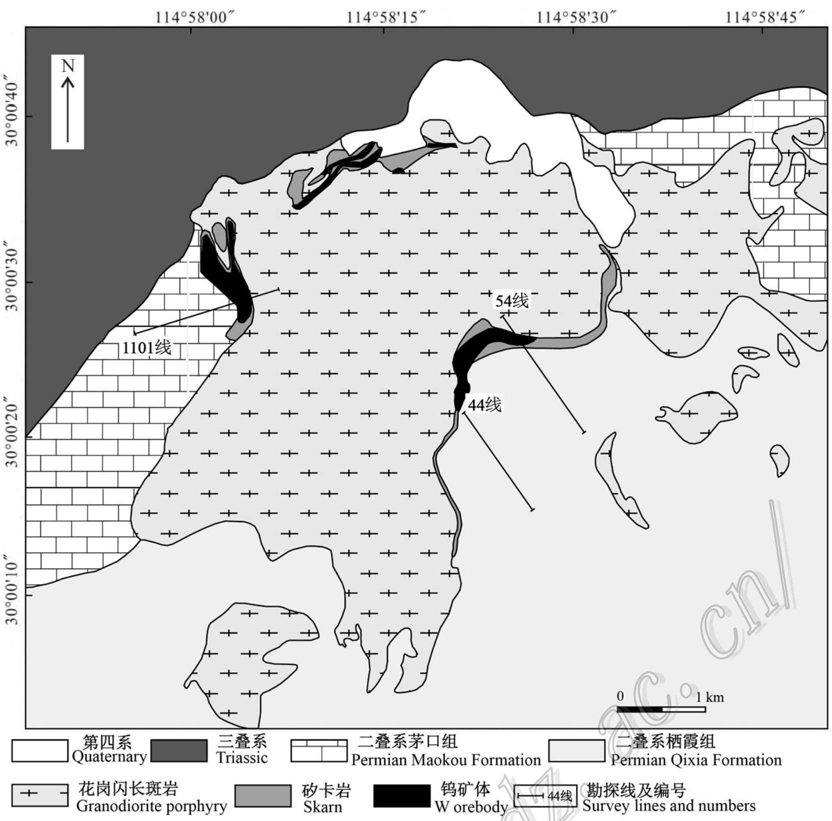

图3 龙角山矿床地质图(据纪云昊等，2019修改)

Fig. 3 Geologic map of the Longjiaoshan deposit (modified after Ji et al., 2019)

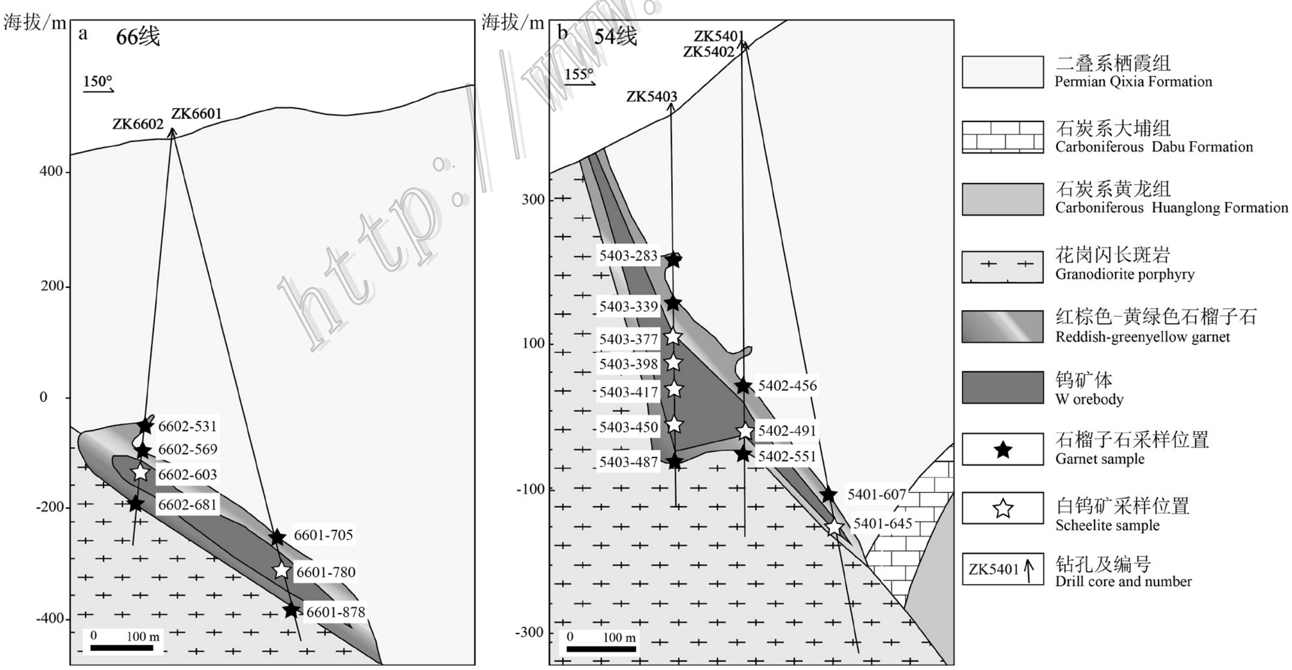

图4 龙角山矿床剖面图(据湖北省第一地质大队，2018修改)

a. 66线剖面图；b. 54线剖面图

Fig.4 Cross section map of the Longjiaoshan deposit (modified after No.1 Geological Party of Hubei Geological Bureau, 2018)

a. Cross section map of 66 Line; b. Cross section map of 54 Line

http://www.kcdz.ac.cn/

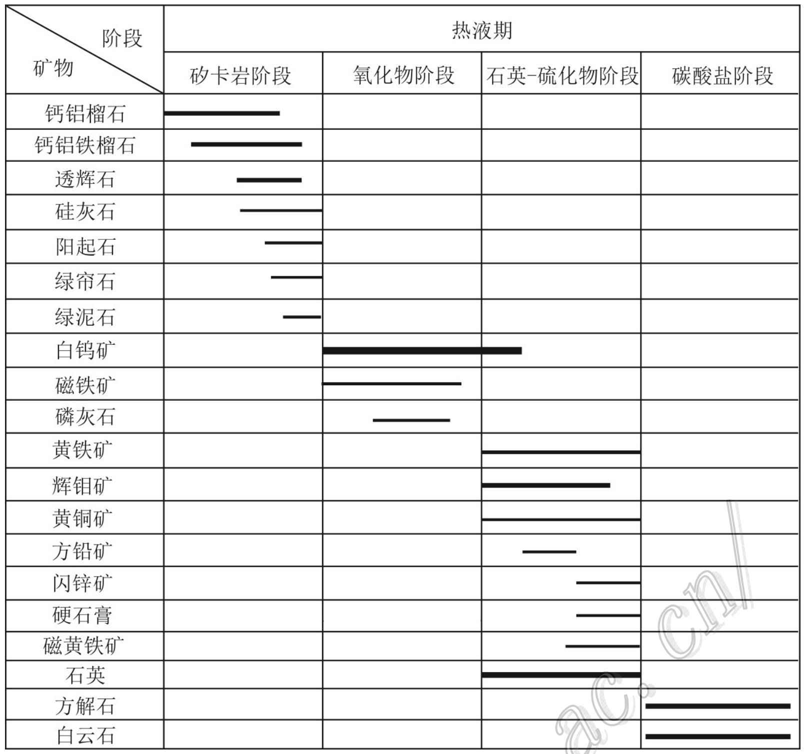

图5　龙角山矿床热液蚀变期次

Fig. 5　Hydrothermal alteration periods of the Longjiaosan deposit

http://www.kcdz.ac.cn/

Ar气和少量N_2气混合后进入质谱仪。测试过程中以NIST SRM 610作为信号漂移矫正,以NIST610作为外标,用无内标法测定主量和微量元素含量。测试数据利用ICPMS Data Cal 9.9离线处理(Liu et al., 2010)。

3　分析测试结果

3.1　阴极发光和面扫描特征

龙角山矿床退蚀变阶段(Sch-1)和石英-硫化物阶段(Sch-2)的白钨矿阴极图像有明显的环带特征,Sch-1呈现明显的环带特征,且颗粒边部CL颜色变浅,据此细分为Sch-1a、Sch-1b和Sch-1c(图7b、e);Sch-2边部环带特征显著,据此分为Sch-2a和Sch-2b(图7h)。

龙角山矿床退蚀变阶段(Sch-1)和石英-硫化物阶段(Sch-2)的白钨矿的面扫描特征显示了不同的元素环带,与阴极发光图像对应,特别是Mo元素,面扫描图像中Mo元素越富集,阴极发光图像中对应的区域灰度越深(图7a~i)。

3.2　主量元素

龙角山矿床石榴子石主量元素特征显示其为钙铝-钙铁榴石系列。矽卡岩阶段的红棕色石榴子石(Grt-1)矽卡岩、黄绿色石榴子石(Grt-2)-辉石矽卡岩和脉状石榴子石-硅灰石矽卡岩中石榴子石(Grt-3)的成分分别为$Adr_{30.6\text{-}84.1}Gro_{13.9\text{-}50.7}Pyr_{1.5\text{-}30.3}$、$Adr_{38.3\text{-}100}Gro_{0.0\text{-}39.4}Pyr_{0.0\text{-}22.4}$和$Adr_{75.3\text{-}100.0}Gro_{0.0\text{-}13.9}Pyr_{0.0\text{-}12.7}$(表1,图8),石榴子石的环带特征与主量元素特征具有很好的耦合型(图8)。前人的研究表明早阶段形成的石榴子石富Al,晚阶段形成的石榴子石富Fe(Einaudi et al., 1981; Nakano et al., 1989; Meinert, 1997; Meinert et al., 2005),与本次实验结果吻合。

龙角山矿床白钨矿主量元素特征显示WO_3和MoO_3呈明显的负相关关系(表2,图9a),且退蚀变阶段白钨矿的$w(MoO_3)$(平均值1.99%)明显高于石英硫化物阶段白钨矿的$w(MoO_3)$(平均值为0.99%)。

3.3　微量元素

龙角山矿床石榴子石微量元素(表3)显示,富集大离子亲石元素(ΣLILE=17184.40×10^{-6}),亏损高场强元素(ΣHFSE=12.13×10^{-6})。上述3类石榴子石的稀土元素呈现明显差异性,Grt-1稀土元素含量最高(ΣREEs=17.60×10^{-6}),Grt-2含量较高(ΣREEs=

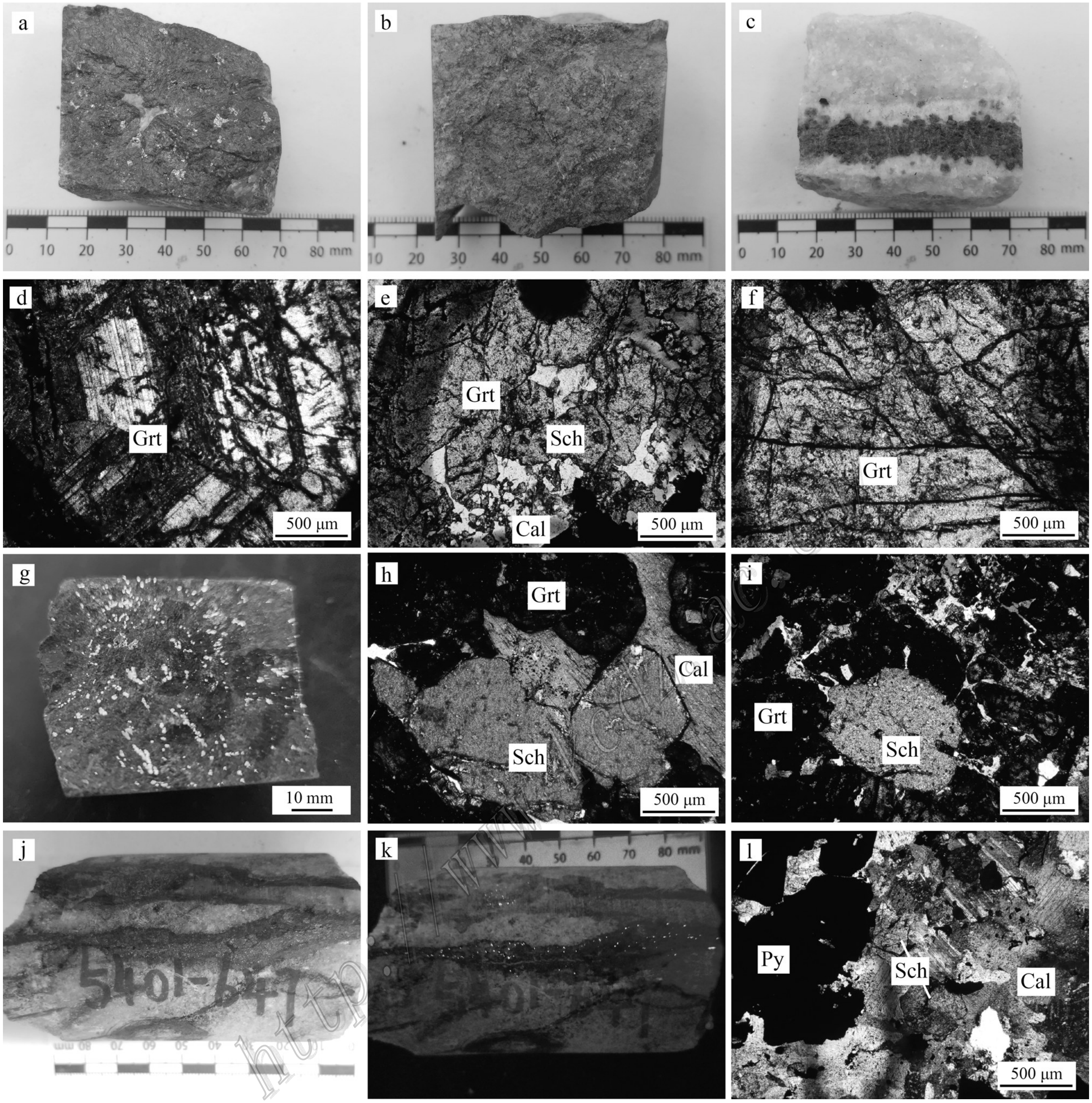

图6 龙角山矿床手标本和镜下照片

a. 红棕色石榴子石内矽卡岩；b. 黄绿色石榴子石-透辉石外矽卡岩；c. 脉状石榴子石-硅灰石外矽卡岩；d. 红棕色石榴子石内矽卡岩（正交偏光）；e. 黄绿色石榴子石-透辉石外矽卡岩（单偏光）；f. 脉状石榴子石-硅灰石外矽卡岩（单偏光）；g. 白钨矿化矽卡岩；h. 白钨矿呈团块状包裹在石榴子石粒间（正交偏光）；i. 白钨矿呈团块状包裹在石榴子石环带（正交偏光）；j. 白钨矿与硫化物共生；k. 白钨矿与硫化物共生（荧光）；l. 白钨矿呈半自形与黄铁矿共生（正交偏光）

Fig. 6 Hand specimen and photomicrographs of the Longjiaoshan deposit

a. Red-brown garnet from endoskarn; b. Yellow-green garnet from exoskarn; c. Veined wollastonite-garnet from exoskarn; d. Photomicrographs of red-brown garnet (orthogonal); e. Photomicrographs of yellow-green garnet (orthogonal); f. Photomicrographs of veined wollastonite-garnet (polarized); g. Hand specimen of scheelite mineralization of skarn; h. Photomicrographs of scheelite metasomatic garnet grain (orthogonal); i. Photomicrographs of scheelite encased in garnet ring (orthogonal); j. Hand specimen of scheelite intergrowth with sulfide; k. Fluorescent image of scheelite intergrowth with sulfide (fluorescence);l. Photomicrographs of subhedral scheelite intergrowth with pyrite (orthogonal)

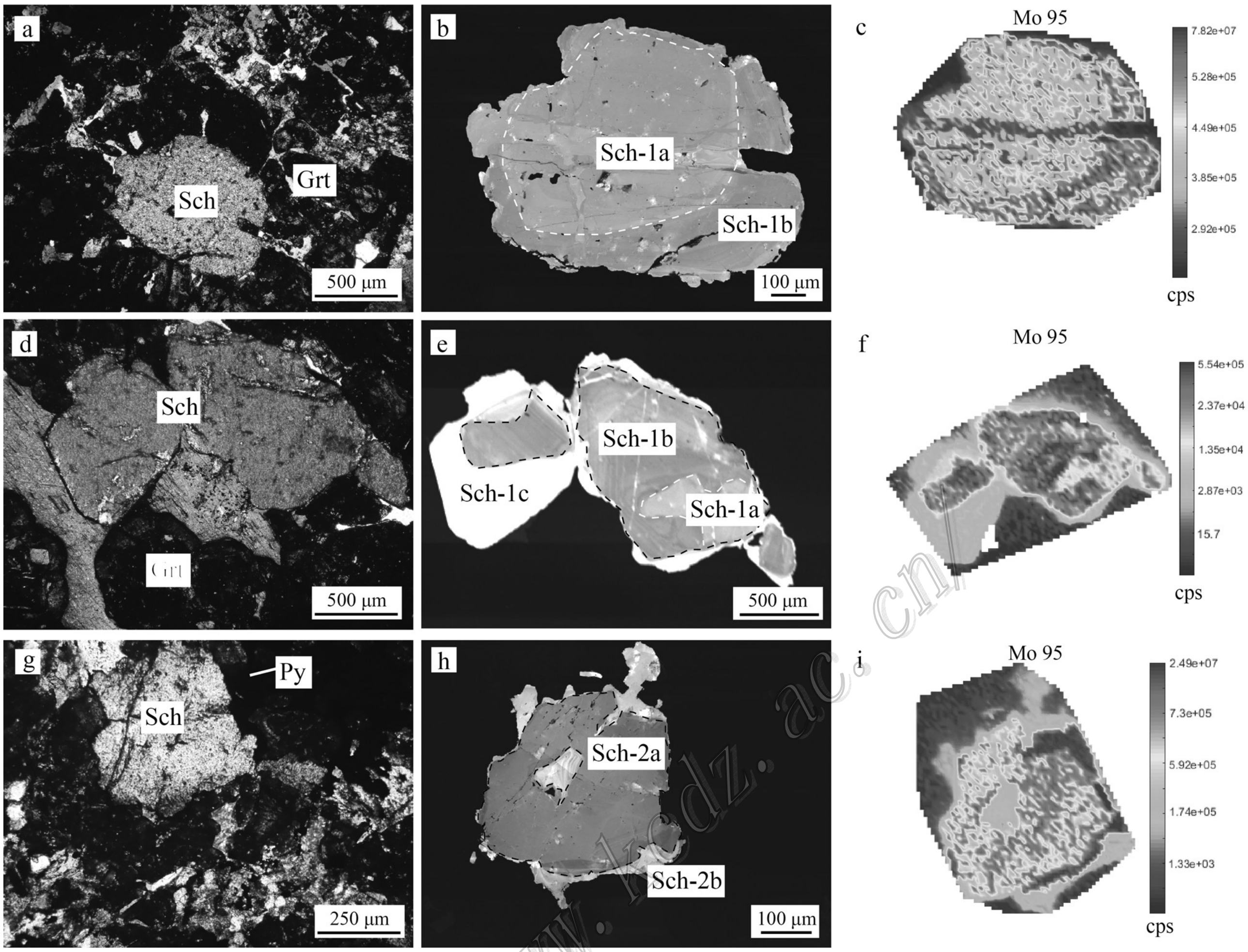

图7　龙角山矿床白钨矿阴极发光和面扫描特征

a. 退蚀变阶段白钨矿(Sch-1)交代石榴子石(Grt)(正交偏光);b. 退蚀变阶段白钨矿(Sch-1)阴极发光图像;c. 退蚀变阶段白钨矿(Sch-1)Mo元素面扫描图像;d. 退蚀变阶段白钨矿(Sch-1)充填石榴子石粒间(正交偏光);e. 退蚀变阶段白钨矿(Sch-1)阴极发光图像;f. 退蚀变阶段白钨矿(Sch-1)Mo元素面扫描图像;g. 自形-半自形石英-硫化物阶段白钨矿(Sch-2);h. 石英-硫化物阶段白钨矿(Sch-2)阴极发光图像;i. 石英-硫化物阶段白钨矿(Sch-2)Mo元素面扫描图像

Fig. 7　Cathodoluminescence and mapping images of scheelite from the Longjiaoshan deposit

a. Retrograde scheelite (Sch-1) metasomasis garnet (Grt) (perpendicular polarized); b. Cathodoluminescence of retrograde scheelite (Sch-1) ; c. Mapping image of retrograde scheelite (Sch-1) of Mo element; d. Retrograde scheelite (Sch-1) metasomatic garnet (perpendicular polarized); e. Cathodoluminescence of retrograde scheelite (Sch-1); f. Mapping image of retrograde scheelite (Sch-1) of Mo element; g. Idiomorphic-semiidiomorphic quartz-sulfide stage scheelite (Sch-2); h. Cathodoluminescence of idiomorphic-semiidiomorphic quartz-sulfide stage scheelite (Sch-2); i. Mapping image of quartz-sulfide scheelite(Sch-2) of Mo element

13.21×10^{-6}),Grt-3稀土元素含量最低(ΣREEs=9.41×10^{-6})。上述3类石榴子石的稀土元素配分模型分布呈现中稀土元素富集、铕正异常的特征(图10a~c)。在Grt-2中,金属元素w(W)(平均值分别22.6×10^{-6})明显高于其他类型的石榴子石。

龙角山矿床白钨矿微量元素亏损大离子亲石元素,如金属元素w(Rb、Ba、U、Th)低于1×10^{-6},但w(Sr)(213.26×10^{-6})明显高于其他大离子亲石元素,且亏损高场强元素,如Zr、Hf、Ta等低于1×10^{-6},但w(Nb)(2.60×10^{-6})明显高于其他高场强元素(表4)。上述2类白钨矿的稀土元素配分模型呈现过渡特征,从退蚀变阶段到石英硫化物阶段白钨矿的LREE含量,逐渐降低且正铕异常逐渐加强(2类白钨矿的δEu平均值分别为0.526和2.423,图10d~f)。

4　讨　论

龙角山矿床中石榴子石和白钨矿含有多种微量

http://www.kcdz.ac.cn/

表 1 龙角山矿床石榴子石电子探针分析结果

Table1 Results of EPAM analysis of garnet from the Longjiaoshan deposit

样品代号	样号	w(B)/%													
		SiO_2	TiO_2	Al2O3	FeO	MnO	MgO	CaO	Na_2O	K_2O	P_2O_5	总和	钙铁榴石	锰铝榴石+镁铝榴石+铁铝榴石	钙铝榴石
Grt-1	5402-551-1	36.71	0	13.75	14.36	0.98	0.51	33.09	0	0	0	99.40	41.11	8.24	50.65
Grt-1	5402-551-10	36.18	0.01	8.07	19.46	1.02	0.02	34.60	0	0	0	99.36	65.87	2.35	31.77
Grt-1	5402-551-11	35.50	0	10.82	19.51	1.37	0.10	31.90	0	0	0	99.20	55.43	10.18	34.38
Grt-1	5402-551-12	35.02	0.08	10.73	19.34	1.68	0.03	32.35	0	0	0	99.23	57.33	9.15	33.52
Grt-1	5402-551-13	36.61	0	7.63	19.88	1.71	0.02	33.37	0	0	0	99.22	66.03	4.59	29.38
Grt-2	5401-607-1	38.64	0	13.07	17.31	0.94	1.74	27.37	0.01	0.21	0	99.29	38.31	22.26	39.44
Grt-2	5401-607-10	35.56	0.05	5.66	22.76	1.56	0.03	33.58	0	0	0	99.20	77.68	3.70	18.63
Grt-2	5401-607-11	35.32	0.01	5.65	23.22	1.12	0.02	33.93	0	0	0	99.27	78.68	3.00	18.32
Grt-2	5401-607-12	36.64	0	4.00	23.90	1.26	0.01	33.40	0	0	0.01	99.22	81.43	2.98	15.59
Grt-2	5401-607-13	34.55	0.23	8.20	22.84	2.17	0.04	31.11	0	0	0	99.14	68.91	11.41	19.69
Grt-3	5403-283-1	34.27	0.41	6.90	24.47	1.85	0.04	31.12	0	0	0	99.06	75.33	10.81	13.86
Grt-3	5403-283-10	43.72	0.01	0.90	20.03	0.83	0.18	33.51	0	0.01	0	99.19	95.11	2.63	2.26
Grt-3	5403-283-11	36.89	0	0.48	27.43	0.58	0.03	33.77	0	0	0	99.18	97.66	1.47	0.88
Grt-3	5403-283-12	11.38	0	10.05	28.79	1.24	3.01	44.32	0.01	0.06	0.01	98.87	100	0	0
Grt-3	5403-283-13	22.50	0	8.35	9.47	0.71	0.25	58.30	0	0	0.01	99.59	100	0	0

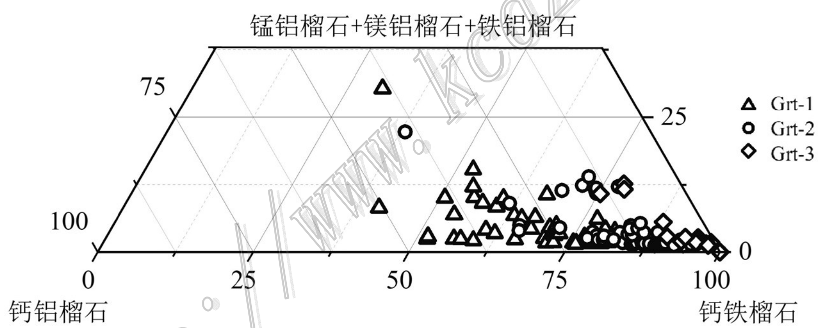

图 8 龙角山矿床石榴子石三角图

Fig. 8 Section of the ternary diagram for garnets from the Longjiaoshan deposit

http://www.kcdz.ac.cn/

元素，如REEs、LILEs(Sr)、HFSEs(Nb)、Mo、Sn、U等，可为岩浆热液体系来源和演化提供证据，如氧逸度、pH值、水岩反应程度等（刘善宝等，2007；Song et al., 2014；Guo et al., 2016；Park et al., 2017；Xiao et al., 2018），因此，本文从上述几个方面分别讨论龙角山矿床的成矿流体特征。

4.1 成矿流体特征

4.1.1 氧逸度

U是一种对氧化还原敏感的元素，因为U^{4+}比U^{6+}更容易替代石榴子石中的钙元素，降低$f(O_2)$可以降低U在流体中的溶解度，从而增加石榴石中的w(U)（Smith et al., 2004；Gaspar et al., 2008）。由于从岩浆中分离出来的流体脉冲不同，形成的石榴子石的生成量不同（Shu et al., 2017），热液流体中初始w(U)相似，石榴子石的w(U)受流体氧化还原状态控制。因此，石榴子石中低w(U)反映了石榴子石形成于氧化环境，而高w(U)则反映了石榴子石形成于还原环境。龙角山Grt-1的w(U)最高，说明它是在相对还原的环境中形成的（图9b）。Grt-3的w(U)最低，表明其形成于氧化环境，这与石榴子石的钙铁榴石的成分变化吻合，表明在矽卡岩阶段成矿流体氧逸度逐渐升高。

Mo也是一种对氧化还原敏感的元素，在氧化条件下以Mo^{6+}的形式迁移并替代W^{6+}进入白钨矿。当

表 2　龙角山矿床白钨矿电子探针分析结果

Table 2　Results of EPAM analysis of scheelite from the Longjiaoshan deposit

样品名称	样号	w(B)/%								
		Na_2O	MgO	SiO_2	CaO	TiO_2	FeO	MoO_3	WO_3	总和
Sch-1a	5403-377-a1	0	0	0.10	20.23	0	0.02	1.92	77.72	99.99
Sch-1a	5403-377-a10	0	0	0.10	19.79	0	0.02	1.56	78.15	99.62
Sch-1a	5403-377-a11	0	0	0.09	19.62	0	0.02	1.46	78.23	99.42
Sch-1a	5403-377-a12	0	0	0.09	19.71	0	0.02	1.46	78.23	99.51
Sch-1a	5403-377-a13	0	0	0.09	20.25	0	0.01	1.50	78.16	100.01
Sch-1b	5403-377-b1	0	0	0.12	20.71	01	0.02	2.73	76.50	100.08
Sch-1b	5403-377-b2	0	0	0.11	20.24	0	0.01	2.62	76.56	99.54
Sch-1b	5403-377-b3	0	0	0.18	20.71	0	0.14	2.88	75.97	99.88
Sch-1b	5403-377-b4	0	0	0.24	21.19	0	0.04	3.02	75.89	100.38
Sch-1b	5403-377-b5	0	0.01	0.30	19.97	0	0.05	2.47	76.80	99.6
Sch-1c	5403-398-c1	0	0	0.09	19.87	0	0.02	0.67	79.55	100.2
Sch-1c	5403-398-c2	0	0	0.09	19.35	0	0.02	0.63	79.77	99.86
Sch-1c	5403-398-c3	0	0	0.07	19.44	0	0.02	1.16	78.52	99.21
Sch-1c	5403-398-c4	0	0	0.08	19.22	0	0.02	0.74	79.20	99.26
Sch-1c	5403-398-c5	0	0	0.09	20.21	0	0.01	0.99	78.79	100.09
Sch-2a	5401-645-a1	0	0.02	0.82	20.23	0	0.04	1.93	77.72	100.76
Sch-2a	5401-645-a10	0	0.13	0.43	20.73	0	0.27	2.30	77.25	101.11
Sch-2a	5401-645-a2	0.01	0.01	0.68	19.59	0	0.04	1.18	78.51	100.02
Sch-2a	5401-645-a3	0	0.01	0.18	19.84	0	0.02	1.01	78.75	99.81
Sch-2a	5401-645-a4	0	0	0.40	19.90	0	0.02	1.15	78.56	100.03
Sch-2b	5401-645-b1	0	0	0.08	19.30	0	0.03	0.55	79.99	99.95
Sch-2b	5401-645-b2	0.01	0	0.09	19.14	0	0.02	0.59	79.92	99.77
Sch-2b	5401-645-b3	0	0	0.08	19.06	0	0.01	0.54	80.07	99.76
Sch-2b	5401-645-b4	0	0	0.08	18.13	0	0.01	0.30	81.05	99.57
Sch-2b	5401-645-b5	0	0	0.07	18.36	0	0.01	0.44	80.90	99.78

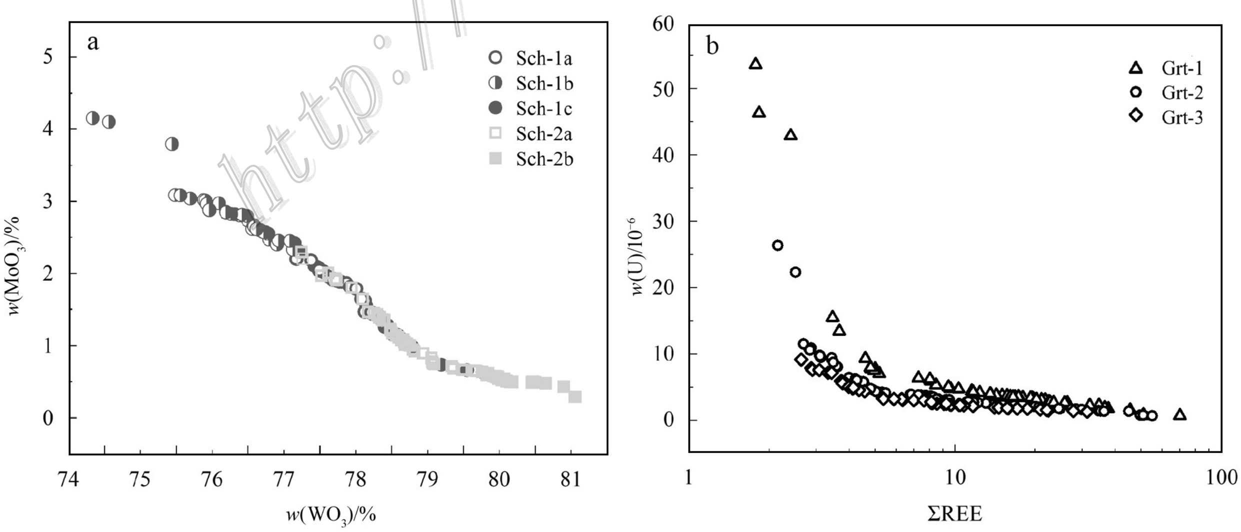

图9　龙角山矿床白钨矿和石榴子石主、微量元素图解

a. 白钨矿 WO_3-MoO_3 图解；b. 石榴子石 ΣREE-U 图解

Fig. 9　Diagrams of major and trace elements of scheelite and garnet from the Longjiaoshan deposit

a. Diagram of WO_3-MoO_3 of scheelite; b. Diagram of ΣREE-U of garnet

http://www.kcdz.ac.cn/

表 3 龙角山矿床石榴子石微量元素分析结果

Table 2 Trace elements of the garnet from the Longjiaoshan deposit

样品	样号	$w(B)/10^{-6}$														
		La	Ce	Pr	Nd	Sm	Eu	Gd	Tb	Dy	Ho	Er	Tm	Yb	Lu	Y
Grt-1	5402-551-1	0.361	4.648	1.415	10.284	3.799	3.765	4.988	1.157	10.163	2.742	10.312	1.791	12.316	1.157	28.466
Grt-1	5402-551-10	6.739	20.594	1.930	4.576	0.236	1.776	0.419	0.047	0.329	0.056	0.211	0.024	0.145	0.020	7.163
Grt-1	5402-551-11	1.978	5.303	0.497	1.749	0.334	0.631	0.266	0.082	0.577	0.115	0.259	0.050	0.355	0.059	0.584
Grt-1	5402-551-12	4.949	9.832	0.878	3.098	0.411	0.497	0.575	0.072	0.454	0.133	0.365	0.044	0.200	0.048	3.512
Grt-1	5402-551-13	3.625	7.323	0.706	2.565	0.296	0.411	0.567	0.065	0.379	0.085	0.322	0.031	0.227	0.029	1.643
Grt-1	5402-551-14	4.020	8.866	0.826	2.908	0.516	0.506	0.437	0.081	0.460	0.138	0.385	0.036	0.263	0.035	2.973
Grt-2	5401-607-1	0.851	2.101	0.336	1.144	0.087	0.340	0.170	0.014	0.107	0.017	0.038	0.005	0.068	0.005	0.005
Grt-2	5401-607-10	0.127	1.029	0.352	2.194	0.799	1.567	0.372	0.034	0.155	0.023	0.038	0.017	0.074	0.012	0.046
Grt-2	5401-607-11	0.804	3.623	0.517	1.238	0.183	0.549	0.188	0.028	0.203	0.051	0.134	0.020	0.112	0.029	0.048
Grt-2	5401-607-12	0.505	1.991	0.181	0.213	0.021	0.116	0.032	0.001	0.016	0.001	0.003	0	0.002	0	0.054
Grt-2	5401-607-13	0.256	4.068	1.072	6.584	2.201	2.404	2.587	0.482	4.002	0.992	3.788	0.638	4.639	0.496	0.059
Grt-2	5401-607-14	0.344	4.211	1.221	6.717	0.847	1.976	0.447	0.051	0.221	0.026	0.062	0.002	0.128	0.005	0.069
Grt-3	5403-283-1	0.431	2.451	0.333	0.458	0.023	0.097	0.066	0.008	0.032	0.006	0.015	0.002	0.008	0.001	1.759
Grt-3	5403-283-10	0.420	5.254	1.176	4.615	0.555	1.407	0.146	0.018	0.111	0.022	0.117	0.013	0.057	0.012	2.644
Grt-3	5403-283-11	0.439	1.803	0.219	0.669	0.128	0.074	0.146	0.025	0.111	0.015	0.050	0.006	0.022	0.003	2.682
Grt-3	5403-283-12	0.162	2.830	0.948	6.539	0.728	2.001	0.474	0.058	0.291	0.059	0.177	0.024	0.137	0.019	2.785
Grt-3	5403-283-13	0.194	1.283	0.368	0.577	0.019	0.340	0.042	0.006	0.030	0.001	0.003	0	0.002	0	2.964
Grt-3	5403-283-14	0.268	3.185	1.085	7.202	0.798	1.883	0.459	0.062	0.322	0.057	0.188	0.025	0.146	0.019	3.005

样品	样号	$w(B)/10^{-6}$													
		Rb	Sr	Zr	Nb	Mo	Cs	Hf	Ta	W	Th	U	REE	ΣLILE	ΣHFSE
Grt-1	5402-551-1	0.222	27.238	0.114	0.005	0.082	0.111	0	0	11.634	0.063	0.232	68.898	27.571	0.414
Grt-1	5402-551-10	0.097	0.546	0.419	1.812	0.128	0	0	0.011	0.970	0.226	1.295	37.102	0.643	3.763
Grt-1	5402-551-11	0.021	29.445	0.087	0.545	0.259	0	0.043	0.014	23.144	0.085	3.724	12.255	29.466	4.498
Grt-1	5402-551-12	0.044	0.108	9.252	5.633	0.145	0.017	0.280	0.029	0.491	0.201	2.576	21.556	0.169	17.971
Grt-1	5402-551-13	0	0.201	0.003	0.003	0.291	0.025	0	0	11.390	0.021	3.031	16.631	0.226	3.058
Grt-1	5402-551-14	0.057	0.147	12.259	7.166	0.243	0.015	0.361	0.037	0.610	0.266	2.808	19.477	0.219	22.897
Grt-2	5401-607-1	12.431	90.975	0.290	0.647	1.092	0.846	0.003	0	4.537	0.080	3.776	5.283	104.252	4.796
Grt-2	5401-607-10	0	0.169	1.826	1.608	0.117	0.009	0.019	0.036	25.612	0.092	3.414	6.793	0.178	6.995
Grt-2	5401-607-11	0.032	0.620	0.310	2.714	0.283	0	0.025	0.016	2.828	0.177	3.300	7.679	0.652	6.542
Grt-2	5401-607-12	0.057	0.138	0	0.021	1.032	0.032	0.021	0.012	11.433	0.001	9.377	3.082	0.227	9.432
Grt-2	5401-607-13	0	0.230	15.640	19.149	0.226	0	0.562	0.386	15.347	0.274	0.962	34.209	0.230	36.973
Grt-2	5401-607-14	0.004	0.461	4.209	0.696	0.211	0	0.094	0.021	1.048	0.226	1.788	16.258	0.465	7.034
Grt-3	5403-283-1	0	0.228	33.266	24.960	0.227	0	1.495	0.810	0.684	0.545	4.785	3.931	0.228	65.861
Grt-3	5403-283-10	0.691	401.064	0.319	2.134	3.013	0.439	0.030	0.019	0.497	0.033	1.458	13.923	402.194	3.993
Grt-3	5403-283-11	0	0.668	0.082	0.107	0.163	0.017	0.012	0.006	0.071	0.046	5.460	3.710	0.685	5.713
Grt-3	5403-283-12	3.699	381.796	0.418	0.232	3.556	0.812	0.018	0.012	0.642	0.091	1.449	14.447	386.307	2.220
Grt-3	5403-283-13	0.078	268.630	0.276	0	0.164	0	0.007	0.002	0.632	0.120	7.399	2.865	268.708	7.804
Grt-3	5403-283-14	1.188	334.386	0.428	0.007	0.354	1.177	0	0	0.036	0.142	1.364	15.699	336.751	1.941

http://www.kcdz.ac.cn/

$f(O_2)$降低时，Mo^{6+}还原为Mo^{4+}，沉淀为辉钼矿（MoS_2）（Rempel et al., 2009；Song et al., 2014）。因次，显示了成矿过程复杂的脉冲式的氧逸度变化特征。

综上所述，龙角山矿床矽卡岩阶段到退蚀变阶段再到石英-硫化物阶段，成矿流体的氧逸度经历了2次先增加后降低的过程，显示了成矿过程复杂的氧逸度变化特征。

4.1.2 pH 值

除氧逸度外，成矿流体pH值的变化也控制了研究区成矿作用的形成，并且显著影响矽卡岩热液中

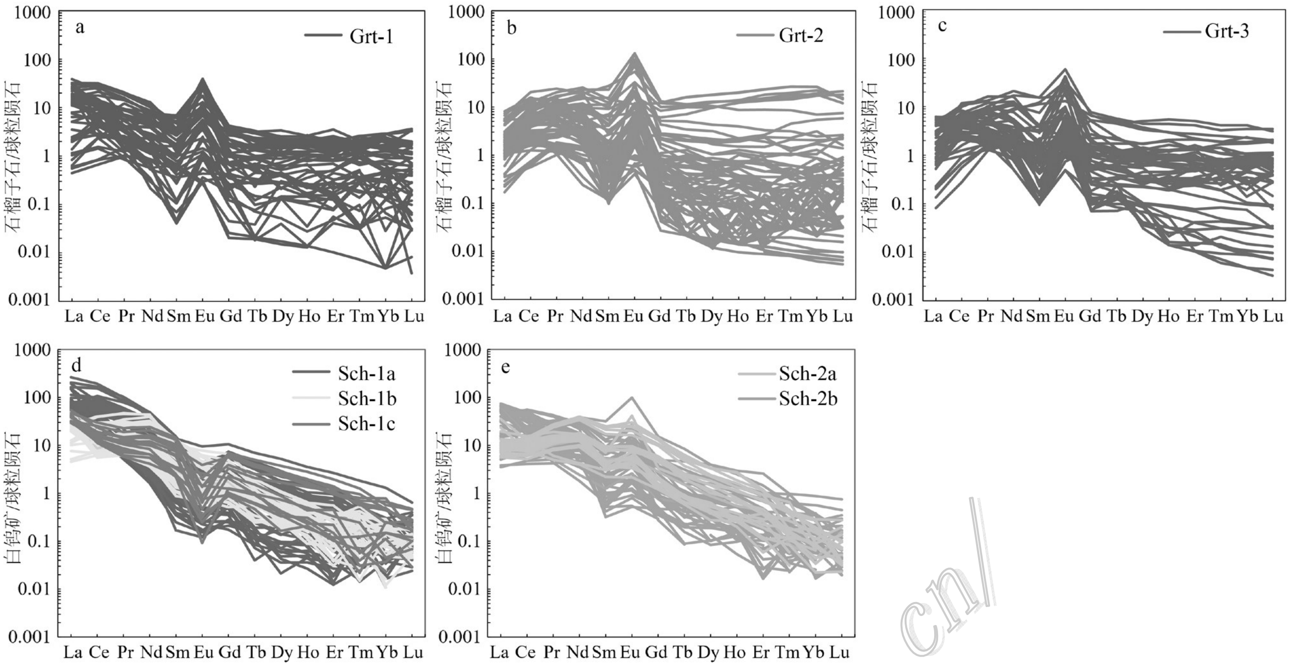

图10　龙角山矿床白钨矿和石榴子石稀土元素配分图解

a. Grt-1稀土元素配分图解；b. Grt-2稀土元素配分图解；c. Grt-3稀土元素配分图解；d. Sch-1稀土元素配分图解；e. Sch-2稀土元素配分图解

Fig. 10　Normalized REE pattern of scheelite and garnet from the Longjiaoshan deposit

a. Normalized REE pattern of Grt-1; b. Normalized REE pattern of Grt-2; c. Normalized REE pattern of Grt-3; d. Normalized REE pattern of Sch-1; e. Normalized REE pattern of Sch-2

http://www.kcdz.ac.cn/

稀土元素的分馏(Bau, 1991)。通常来说，在中性条件下，石榴子石的稀土元素模式为富集重稀土元素和亏损轻稀土元素，且Eu呈负异常或无异常；在中等酸性pH值条件下，稀土元素模式更多地受Cl^-的控制，Cl^-的存在可以增强除REE^{3+}外的可溶Eu^{2+}($EuCl_4^{2-}$为主)离子的稳定性，并导致明显的Eu正异常，且富集轻稀土元素、亏损重稀土元素(Bau, 1991；Gaspar et al., 2008；Zhang et al., 2017)。在龙角山矿床中，Grt-1、Grt-2和Grt-3均表现出轻稀土元素富集、重稀土元素亏损、铕正异常，且稀土元素含量逐渐减少的特征(图10)，说明在矽卡岩阶段，成矿流体热液pH值较稳定，为酸性条件。低pH值水溶液可以携带高浓度的钨(Wood et al., 2000；Wang et al., 2019)，即pH值的任何增加都可能导致流体中钨的饱和，从而导致白钨矿的沉淀。pH值的改变的成矿系统在退蚀变阶段发生，此阶段成矿流体与碳酸盐岩类围岩反应程度达到峰值，这一过程将增加成矿流体pH值(Legros et al., 2020)。

白钨矿的正铕异常特征为成矿流体与富钙质岩石或矿物反应提供了证据，这是由于富钙质岩石(如灰岩)或矿物(如斜长石)中Eu以+2价离子形式存在，且Eu^{2+}较Eu^{3+}更易进入白钨矿晶格(Shannon, 1976；Cottrant, 1981；Raimbault et al., 1993；Ghaderi et al., 1999；Brugger et al., 2008)，因此，正铕异常显示了热液流体与围岩发生充分反应(Sun et al., 2017；Wang et al., 2017；Zhang et al., 2018；Wu et al., 2019)。龙角山矿床2类白钨矿显示铕负异常减弱铕正异常增加的特征，这与上文前人提出的成矿阶段热液pH增加相吻合。综上所述，龙角山矿床矽卡岩阶段到退蚀变阶段再到石英-硫化物阶段，成矿流体的pH值逐渐增加，而非在退蚀变阶段(成矿阶段)达到峰值，因此，pH值不是影响白钨矿沉淀的主要因素。

4.1.3　水岩反应程度

矽卡岩的形成是一个动态过程，包括不同阶段的热液活动和岩浆热液流体的持续演化(Meinert, 1997；Meinert et al., 2005)。Y作为一种特殊的稀土元素，在平衡体系中，Y与REE存在正相关关系；在非平衡体系中，Y与REEs无正相关性且富集轻稀土元素(Gaspar et al., 2008；Yardley et al., 1991)。本文测的Grt-1稀土元素总量与Y存在正相关关系，而Grt-2、Grt-3稀土元素总量与Y不存在正相关关系(图11a)，反映了随着石榴子石的结晶由平

表4 龙角山矿床白钨矿微量元素分析结果

Table 4 Trace elements of the scheelite from the Longjiaoshan deposit

样品	样号	w(B)/10⁻⁶														
		La	Ce	Pr	Nd	Sm	Eu	Gd	Tb	Dy	Ho	Er	Tm	Yb	Lu	Y
Sch-1a	5403-398-a1	24.253	43.611	3.387	7.917	0.572	0.129	0.373	0.048	0.169	0.046	0.063	0.005	0.009	0.004	3.510
Sch-1a	5403-398-a2	30.160	78.350	6.862	18.629	1.543	0.212	0.965	0.080	0.355	0.053	0.117	0.015	0.036	0.008	0.894
Sch-1a	5403-398-a3	10.700	7.317	1.250	4.885	0.523	0.025	0.329	0.020	0.055	0.013	0.042	0	0.019	0	1.382
Sch-1b	5403-398-b1	12.362	37.142	3.645	9.308	0.952	0.137	0.674	0.056	0.230	0.026	0.061	0.001	0.028	0	0.397
Sch-1b	5403-398-b10	8.863	4.470	0.764	2.463	0.282	0.053	0.133	0.026	0.092	0.015	0.083	0.011	0.053	0.005	0.077
Sch-1b	5403-398-b2	16.431	46.830	4.251	11.166	0.836	0.176	0.654	0.057	0.263	0.034	0.058	0.005	0.017	0.002	0.595
Sch-1c	5403-398-c1	23.922	26.004	1.155	2.282	0.243	0.022	0.179	0.019	0.071	0.017	0.032	0.001	0.008	0.002	1.348
Sch-1c	5403-398-c2	19.207	18.027	0.906	1.987	0.180	0.026	0.262	0.018	0.081	0.010	0.029	0	0.008	0.001	0.183
Sch-1c	5403-398-c3	17.489	16.754	0.784	1.296	0.098	0.024	0.174	0.005	0.057	0.015	0.013	0.001	0	0	0.125
Sch-2a	5401-645-a1	1.714	5.816	1.250	6.339	1.788	1.986	1.175	0.102	0.377	0.064	0.101	0.006	0.019	0.005	0.645
Sch-2a	5401-645-a10	12.621	45.216	5.177	14.872	1.474	0.414	0.917	0.091	0.312	0.068	0.098	0.005	0.016	0	0.713
Sch-2a	5401-645-a2	9.514	15.972	1.659	4.761	0.300	0.143	0.132	0	0.043	0.004	0.005	0.003	0.012	0	0.487
Sch-2b	5401-645-b1	16.314	43.457	4.862	13.178	0.123	0.162	0.107	0	0	0	0	0	0	0	1.342
Sch-2b	5401-645-b2	17.243	15.078	0.954	4.612	1.254	0.836	0.860	0.072	0.506	0.073	0.143	0.013	0.072	0.001	0.318
Sch-2b	5401-645-b3	18.088	14.761	0.703	2.264	0.412	0.317	0.398	0.039	0.201	0.020	0.037	0.007	0.028	0.002	0.564

样品	样号	w(B)/10⁻⁶												δEu	Zr/Hf	Rb/Sr	Nb/La
		Rb	Sr	Zr	Nb	Mo	Cs	Hf	Ta	W	Th	U	Nb+Ta				
Sch-1a	5403-398-a1	0.059	205.554	0	2.759	9590.008	0.015	0	0.048	620670	0.040	0.025	2.807	0.800	-	0	0.114
Sch-1a	5403-398-a2	0.004	186.397	0.012	5.444	9543.613	0	0	0.102	620800	0.028	0.007	5.546	0.495	-	0	0.180
Sch-1a	5403-398-a3	0	187.094	0.004	2.024	9445.386	0	0	0.052	621128	0.054	0.010	2.076	0.175	-	0	0.189
Sch-1b	5403-398-b1	0.079	246.226	0.037	1.072	19678.654	0	0	0.021	602261	0.011	0.029	1.093	0.499	-	0	0.087
Sch-1b	5403-398-b10	0	192.846	0.028	2.075	15948.468	0	0.003	0.045	611403	0.006	0.017	2.120	0.730	8.160	0	0.234
Sch-1b	5403-398-b2	0.068	240.857	0.013	0.978	19747.815	0	0.005	0.009	602539	0.012	0.652	0.987	0.701	2.715	0	0.060
Sch-1c	5403-398-c1	0.047	137.084	0.012	3.861	4417.656	0.021	0.003	0.013	630887	0.003	0.018	3.875	0.303	3.342	0	0.161
Sch-1c	5403-398-c2	0	197.078	0.011	1.220	4214.091	0	0	0.012	632591	0.009	0.018	1.233	0.361	-	0	0.064
Sch-1c	5403-398-c3	0.007	177.385	0.016	1.056	7692.262	0.024	0.006	0.013	622737	0.015	0.034	1.069	0.551	2.421	0	0.060
Sch-2a	5401-645-a1	0.241	298.483	0.143	3.225	12828.729	0.055	0.010	0.096	616078	0.003	0.093	3.321	3.944	14.098	0.001	1.882
Sch-2a	5401-645-a10	0.206	458.288	0.018	2.286	15254.013	0.085	0.005	0.077	612467	0.005	0.026	2.363	1.015	3.463	0	0.181
Sch-2a	5401-645-a2	0.261	250.737	0.072	3.340	7813.445	0.079	0.005	0.090	622659	0.024	0.053	3.431	1.892	13.309	0.001	0.351
Sch-2b	5401-645-b1	0.460	158.760	0.005	2.244	3667.033	0.021	0	0.016	634348	0.019	0.076	2.260	4.230	-	0.003	0.138
Sch-2b	5401-645-b2	0.405	164.614	0	2.623	3897.073	0.065	0.002	0.011	633808	0.018	0.004	2.634	2.333	0	0.002	0.152
Sch-2b	5401-645-b3	0.025	147.001	0.008	1.643	3610.831	0	0	0.012	634870	0.010	0.002	1.655	2.360	-	0	0.091

注：比值单位为1。

http://www.kcdz.ac.cn/

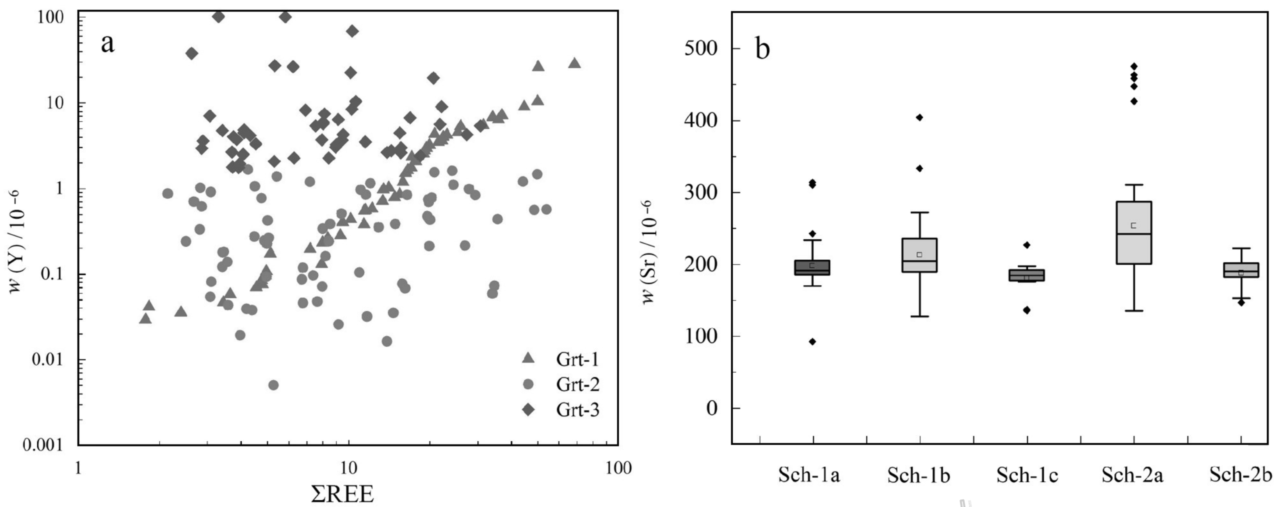

图 11　龙角山矿床石榴子石和白钨矿图解

a. 石榴子石ΣREE和Y元素图解;b. 白钨矿Sr元素图解

Fig. 11　Diagrams of scheelite and garnet from the Longjiaoshan deposit

a. Diagram of ΣREE and Y of garnet; b. Diagram of Sr of scheelite

衡状态向非平衡状态转变,即水岩反应程度逐渐增加,由封闭的热液系统逐步向开放的热液系统过渡(Park et al., 2017),矽卡岩从反应矽卡岩(扩散)演化为交代矽卡岩(渗透)(Meinert et al., 2005),而开放体系石榴子石以富Fe为特征(Gaspar et al., 2008),这与本文所观察到的Grt-3钙铁榴石成分高($Adr_{75.3\text{-}100.0}Gro_{0.0\text{-}13.9}Pyr_{0.0\text{-}12.7}$,图8)相吻合。这一过程增加了矽卡岩蚀变灰岩的孔隙度和渗透率,允许进一步的热液流动,从而增加了体系的水岩比,且对应形成的富Fe石榴子石稀土元素总含量逐渐减少,这一现象在龙角山矿床石榴子石的稀土元素特征中得到印证(表3),且Sch-1和Sch-2的w(Sr)呈现增加的趋势(图11b),同时,由于热液矿物生长时物理和化学条件的波动,晶体内部会产生微小的缺陷,而CL或BSE图像可以精准的反映矿物的微观形貌学特征(Rusk et al., 2002; 2008; Putnis, 2009; Han et al., 2020),单个白钨矿颗粒中不同灰度的区域代表不同世代白钨矿在不同物理和化学条件下的流体平衡状态。在Sch-1a和Sch-2a颗粒的周边均表现不规则生长特征(即Sch-1b、Sch-1c和Sch-2b)(图7a~i),且主成矿阶段Sch-1的不规则生长环带比Sch-2更发育,这也反映了主成矿阶段(退蚀变阶段)水岩反应程度达到峰值。

4.2　龙角山矿床钨的富集沉淀机制

前人研究表明,钨在热液中的富集和迁移机制受控于流体物理化学条件(温度、压力、氧逸度、pH值)的改变(Bai et al., 1999; Wood et al., 2000; Zajacz et al., 2008);控制钨的沉淀机制主要有:温压降低(Ni et al., 2015; Chen et al., 2018)、水岩反应(Lecumberri et al., 2017)、流体混合(Wei et al., 2012; Legros et al., 2019; Pan et al., 2019)、流体不混溶(Korges et al., 2018; 王国光等, 2020),如大湖塘钨铜多金属矿床成矿流体发生强烈的水岩反应导致矿质沉淀(Sun et al., 2017)。柿竹园钨锡多金属矿床大气降水参与成矿体系是白钨矿沉淀的主要机制(祝新友等, 2015)。南泥湖钨钼矿床经历了流体混合和流体不混溶作用(Yang et al., 2012; 蒋少涌等, 2020)。淘锡坑钨矿和岩前钨矿成矿流体的不混溶作用是矿质沉淀的主要原因(鲁麟等, 2018; 刘畅等, 2018)。

在上述4种钨的沉淀机制中,降温减压过程可能不是白钨矿矿床形成的有效因素(Foster, 1977; Wood et al., 2000),因为100~500℃范围的白钨矿溶解度随着温度降低而增加。由前文(4.1.1)可知,龙角山矿床成矿流体氧逸度变化复杂,存在多次升高降低的过程。而流体混合很可能伴着的$f(O_2)$和pH值增加,温度降低(Linnen et al., 1994; Singoyi et al., 2001; Wei et al., 2012),因此,龙角山白钨矿氧逸度的多次升高很可能反映了有新的流体混入,前人研究也表明龙角山矿床成矿流体存在大气水和有机质混入(Lei et al., 2018),因此,流体混合是龙角山钨矿

床矿质沉淀的重要原因之一。

由前文(4.1.2)可知,pH 值不是影响龙角山矿床白钨矿沉淀的主要因素。而流体不混溶则导致压力降低和 pH 值升高(Lu et al., 2003; Korges et al., 2017; Orhan, 2017; Soloviev et al., 2017)。因此,龙角山矿床的流体不混溶作用可忽略。由前文(4.1.3)可知,水岩反应在龙角山矿床主成矿阶段达到峰值,有利于形成白钨矿。水岩反应主要伴随着热液非极性挥发分的加入、Ca 离子富集和 pH 值增加(Gibert et al., 1992; O'Reilly et al., 1997),通常被认为是形成钨矿床的关键机制(Lecumberri et al., 2017)。

综上所述,流体混合和水岩反应是控制龙角山矿床钨沉淀的主要机制,二者协同控制白钨矿沉淀成矿。流体混合作用被认为是形成具有异常高品位钨矿床的主要沉淀机制(Wei et al., 2012; Korges et al., 2017)。水岩反应也是形成大型、超大型钨多金属矿床的重要过程(如大湖塘钨铜多金属矿床,Peng et al., 2018),通过本次工作可知,龙角山钨矿床的矿质沉淀机制兼具流体混合和水岩作用,该矿区具有成大矿、富矿的潜质。

5 结 论

(1) 龙角山矿床矽卡岩阶段的红棕色石榴子石(Grt-1)矽卡岩、黄绿色石榴子石(Grt-2)-辉石矽卡岩和脉状石榴子石-硅灰石矽卡岩中石榴子石(Grt-3)的成分分别为 $Adr_{30.6\text{-}84.1}Gro_{13.9\text{-}50.7}Pyr_{1.5\text{-}30.3}$、$Adr_{38.3\text{-}100}Gro_{0.0\text{-}39.4}Pyr_{0.0\text{-}22.4}$ 和 $Adr_{75.3\text{-}100.0}Gro_{0.0\text{-}13.9}Pyr_{0.0\text{-}12.7}$,且富集大离子亲石元素,亏损高场强元素,具有富集轻稀土元素、亏损重稀土元素、铕正异常的特征。

(2) 龙角山矿床矽卡岩阶段石榴子石 U 含量逐渐降低,且与钙铁榴石的成分变化吻合,表明在矽卡岩阶段成矿流体氧逸度逐渐升高;退蚀变阶段到石英-硫化物阶段白钨矿 w(Mo)先升高、后降低,对应的氧逸度先增加后降低,显示了成矿过程复杂的脉冲式的氧逸度变化特征。

(3) 龙角山矿床退蚀变阶段和石英-硫化物阶段对应形成的白钨矿显示铕负异常减弱、铕正异常增加的变化特征,表明成矿流体的 pH 值逐渐增加,而非在退蚀变阶段(主成矿阶段)达到峰值,因此,pH 值不是影响白钨矿沉淀的主要因素。

(4) 龙角山矿床矽卡岩阶段 Grt-1 稀土元素总量与 Y 存在正相关关系,Grt-2 和 Grt-3 稀土元素总量与 Y 不存在正相关关系,且 Grt-3 富 Fe,表明随着石榴子石的结晶由热液平衡状态向非平衡条件件转变,即水岩反应程度逐渐增加;退蚀变阶段(主成矿阶段)Sch-1 的不规则生长环带比石英硫化物阶段 Sch-2 更发育,表明主成矿阶段水岩反应程度达到峰值,水岩反应是控制该矿床矿质沉淀的重要因素。

(5) 流体混合和水岩反应是控制龙角山矿床钨沉淀的主要机制,二者协同控制白钨矿沉淀成矿,龙角山矿区具有成大矿、富矿的潜质。

致 谢 野外地质工作期间得到了湖北省地质局第一地质大队杨伟卫院长等多位工程师的大力支持和帮助。合肥工业大学资源与环境工程学院汪方跃副教授在电镜分析过程中提供了热情的指导。审稿专家为本文提出了宝贵的修改意见。在此一并对上述人员志以谢忱!

http://www.kcdz.ac.cn/

References

Bai T B and Van Groos A F K. 1999. The distribution of Na, K, Rb, Sr, Al, Ge, Cu, W, Mo, La, and Ce between granitic melts and coexisting aqueous fluids[J]. Geochimica et Cosmochimica Acta, 63 (7): 1117-1131.

Bau M. 1991. Rare-earth element mobility during hydrothermal and metamorphic fluid-rock interaction and the significance of the oxidation state of europium[J]. Chemical Geology, 93: 219-230.

Brugger J, Bettiol A A, Costa S, Lahaye Y, Bateman R, Lambert D D and Jamieson D N. 2000. Mapping REE distribution in scheelite using luminescence[J]. Mineralogical Magazine, 64: 891-903.

Campbell L S and Henderson P. 1997. Apatite paragenesis in the Bayan Obo REE-Nb-Fe ore deposit, Inner Mongolia, China[J]. Lithos, 42 (1-2): 89-103.

Chang Y F, Liu X P and Wu Y C. 1991. The copper-iron belt of the middle and Lower reaches of Yangtze river[M]. Beijing: Geological Publishing House. 1-380(in Chinese).

Chen X F, Zhou T F, Zhang D Y, Xiong Z Y, Lü QL, Yuan F, Ren Z and Fan Y. 2017. Geochronoligy, geochemistry and geological characteristics of the granite porphyry beneath Guilinzheng Mo deposit, Chizhou, southern Anhui[J]. Acta Petrologica Sinica, 33(10): 3200-3216(in Chinese with English abstract).

Chen X L, Liang H Y, Richards J P, Huang W T, Zhang J, Wu J and Sotiriou P. 2018. Age and granite association of skarn W mineralization at Niutangjie district, South China Block[J]. Ore Geology Reviews, 102: 268-283.

Cottrant J F. 1981. Cristallochimie et geochimie des tarres dans la scheelite: Application a quelquesgisementsfrancais (Doctoral degree thesis)[D]. France: University of Paris. 1-239.

Crowe D E, Riciputi L R, Bezenek S and Ignatiev A. 2001. Oxygen isotope and trace element zoning in hydrothermal garnets: Windows into large-scale fluid-flow behavior[J]. Geology, 29(6): 479-482.

Ding L X, Huang G C and Xia J L. 2014. Petrogenesis of the LongjiaoshanFujiashanporphyritic intrusion in southeastern Hubei Province and implications for Cu-W mineralization[J]. Acta Geologica Sinica,88(8):1513-1527(in Chinese with English abstract).

Ding N. 2012. Metallogenic regularity of tungsten deposits in Anhui Province(master thesis) [D]. Surpervisor: Zhou T F and Du J G. Hefei: Hefei University of Technology. 1-155(in Chinese).

Einaudi M T, Meinert L D and Newberry R J. 1981. Skarn deposits[J]. Econ. Geol., 75: 317-391.

Fan Y, Zhou T F, Yuan F, Zhang L J, Qian B, Ma L, Xie J and Yang X F. 2011. Geochronology of porphyry-like type iron deposits in Ning-Wu Basin：Evidence from ^{40}Ar-^{39}Ar phlogopite dating[J]. Acta Geologica Sinica, 85(5): 810-820(in Chinese with English abstract).

Foster R P. 1977. Solubility of scheelite in hydrothermal chloride solutions[J]. Chemical Geology, 20(77): 27-43.

Gaft M, Panczer M, Uspensky G and Reisfeld E. 1999. Laser-induced time-resolved luminescence of rare-earth elements in scheelite[J]. Mineralogical Magazine, 63(2): 199-210.

Gaspar M, Knaack C, Meinert L D and Moretti R. 2008. REE in skarn systems: A LA-ICP-MS study of garnets from the Crown Jewel gold deposit[J]. Geochimica et Cosmochimica Acta, 72(1): 185-205.

Ghaderi M J, Palin M, Campbell I H and Sylvester P J. 1999. Rare earth systematic in scheelite from hydrothermal gold deposits in the Kalgoolie-Norseman Region, western Australia[J]. Econ. Geol., 94: 423-438.

Gibert F, Moine B, Schott J and Dan durand J L. 1992. Modeling of the transport and deposition of tungsten in the scheelite-bearing calc-silicate gneisses of the Montagne Noire, France[J]. Contributions to Mineralogy and Petrology, 112(2-3): 371-384.

Giere R. 1996. Formation of rare earth minerals in hydrothermal systems[J]. Rare Earth Minerals Chemistry Origin & Ore Deposits, (23): 105-150.

Goldmann S, Melcher F, Gäbler H E, Dewaele S, Clercq F D and Muchez P. 2013. Mineralogy and trace element chemistry of ferberite/reinite from tungsten deposits in Central Rwanda[J]. Minerals, 3 (2): 121-144.

Götze J and Kempe U. 2002. Preface-special Issue: Cathodoluminescence in the geosciences[J]. Mineralogy and Petrology, 76(3-4): 165-166.

Guo Z, Li J, Xu X, Song Z Y, Dong X Z, Tian J, Yang Y C, She H Q, Xiang A P and Kang Y J. 2016. Sm-Nd dating and REE composition of scheelite for the Honghuaerji scheelite deposit, Inner Mongolia, northeast China[J]. Lithos, 261: 307-321.

Han J, Chen H, Hong W, Pete H, Chu G B, Zhang L and Sun S Q. 2020. Texture and geochemistry of multi-stage hydrothermal scheelite in the Tongshankou porphyry-skarn Cu-Mo(-W) deposit, eastern China: Implications for ore-forming process and fluid metasomatism[J]. American Mineralogist, 105: 945-954.

Harlaux M, Mercadier J, Marignac C, Peiffert C, Cloquet C and Cuney M. 2018. Tracing metal sources in peribatholitic hydrothermal W deposits based on the chemical composition of wolframite: The example of the Variscan French Massif Central[J]. Chemical Geology, 479: 58-85.

Hazarika P, Mishra B and Pruseth K L. 2016. Scheelite, apatite, calcite and tourmaline compositions from the Late Archean Hutti orogenic gold deposit: Implications for analogous two stage ore fluids[J]. Ore Geology Reviews, 72: 989-1003.

Huang X W, Gao J F, Qi L and Zhou M F. 2015. In-situ LA-ICP-MS trace elemental analyses of magnetite and Re-Os dating of pyrite: The Tianhu hydrothermally remobilized sedimentary Fe deposit, NW China[J]. Ore Geology Reviews, 65: 900-916.

Ji Y H, Xie G Q, Zhu Q Q, Sun X F and Li X H. 2019. Influence of carbonaceous strata on skarn tungsten deposits: A case study of Fujiashan deposit in eastern Hubei Province[J]. Mineral Deposits, 38 (4): 917-934(in Chinese with English abstract).

Jiang S Y, Zhao K D, Jiang H, Su H M, Xiong S F, Xiong Y Q, Xu Y M, Zhang W and Zhu L Y. 2020. Spatiotemporal distribution, geological characteristics and metallogenic mechanism of tungsten and tin deposits in China: An overview[J]. Chinese Science Bulletin, 65: 3730-3745(in Chinese with English abstract).

Korges M, Weis P, Lüders V and Laurent O. 2017. Depressurization and boiling of a single magmatic fluid as a mechanism for tin-tungsten deposit formation[J]. Geology, 46(1): 75-78.

Lecumberri-Sanchez P, Vieira R, Heinrich CA, Pinto F and Wälle M. 2017. Fluid-rock interaction is decisive for the formation of tungsten deposits[J]. Geology, 45(7): 579-582.

Legros H, Richard A, Tarantola A, Kouzmanov K, Mercadier J V ennemann T, Marignac C, Cuney M, Wang R C, Charles N, Bally L and Lespinasse M Y. 2019. Multiple fluids involved in granite-related W-Sn deposits from the world-class Jiangxi Province (China)[J]. Chemical Geology, 508: 92-115.

Legros H, Lecumberri-Sanchez P, Elongo V, Laurent O, Falck H, Adlakha E and Chelle-Michou C. 2020. Fluid evolution of the Cantung tungsten skarn, northwest Territories, Canada: Differentiation and fluid-rock interaction[J]. Ore Geology Review, 127: 103866.

Lei X F, Duan D F and Jiang S Y. 2018. Ore-forming fluids and isotopic (H-O-C-S-Pb) characteristics of the Fujiashan-Longjiaoshan skarn W-Cu-(Mo) deposit in the Edong district of Hubei Province, China[J]. Ore Geology Reviews, 102: 386-405.

Li X Y, Gao J F, Zhang R Q, Lu J J, Chen W H and Wu J W. 2018. Origin of the Muguayuan veinlet-disseminated tungsten deposit, South China: Constraints from in-situ trace element analyses of scheelite[J]. Ore Geology Reviews, 99: 180-194.

Linnen R L and Williams-Jones A E. 1994. The evolution of pegmatitehosted Sn-W mineralization at NongSua, Thailand: Evidence from fluid inclusions and stable isotopes[J]. Geochimica et Cosmochimica Acta, 58(2):735-747.

Liu C, Zhao Z, Lu L N, Zeng Z L, Liu C H and Xu H. 2018. Metallogenic fluid study of the Yanqianskarn type tungsten deposit in eastern Nanlingregion[J]. Acta Geologica Sinica, 92(12): 2485-2507(in Chinese with English abstract).

Liu J, Li W C, Zhu X P, Li C, Zhou Q and Yang F C. 2020. Origin and evolution of ore-forming fluids of the Larong W-(Mo) deposit, eastern Tibet: Constraints from fluid inclusions, H-O isotopes, and scheelite geochemistry[J]. Ore Geology Reviews, 124: 1368-1387.

Liu S B, Wang D H, Chen Y C, Xu J X, Zeng Z L, Ying L J and Wang C H. 2007. SHRIMP dating of Tianmenshangranite pluton and granite-porphyry dyke in southern Jiangxi Province, eastern Nanlingregion, and its significance[J]. Acta Geologica Sinica, 81(7): 972-978(in Chinese with English abstract).

Liu Y, Hu Z, Zong K, Gao C, Gao S, Xu J and Chen H. 2010. Reappraisement and refinement of zircon U-Pb isotope and trace element analyses by LA-ICP-MS[J]. Chinese Science Bulletin, 15: 1535-1546.

Lu H Z, Liu Y M, Wang C L, Xu Y Z and Li H Q. 2003. Mineralization and fluid inclusion study of the Shizhuyuan W-Sn-Bi-Mo-F skarn deposit, Hunan Province, China[J]. Econ. Geol., 98(5): 955-974.

Lu L, Liang T, Ren W Q, Zhao Z, Liu S B and Chen Z H. 2018. Mineralization mechanism of Taoxikeng quartz vein type tungsten deposit in southern Jiangxi Province: Evidence from fluid inclusions study[J]. Mineral Deposits, 37(6): 1260-1280(in Chinese with English abstract).

Lü Q T, Shi D N, Liu ZD, Zhang Y Q, Dong S W and Zhao J H. 2015. Crustal structure and geodynamics of the Middle and Lower reaches of Yangtze metallogenic belt and neighboring areas: Insights from deep seismic reflection profiling[J]. Journal of Asian Earth Sciences, 114: 704-716.

Lü Q T, Meng G X, Zhang K, Liu Z D, Yan J Y, Shi D N, Han J G and Gong X J. 2021. The lithospheric architecture of the Lower Yangtze Metallogenic belt, East China: Insights into an extensive Fe-Cu mineral system[J]. Ore Geology Reviews, 132: 103989.

Macrae C M, Wilson N C and Brugger J. 2009. Quantitative cathodoluminescence mapping with application to a Kalgoorlie scheelite[J]. Microscopy and Microanalysis the Official Journal of Microscopy Society of America Microbeam Analysis Society Microscopical Society of Canada, 15(3): 222-230.

Mair J L. 2006. Geochemical constraints on the genesis of the Scheelite dome intrusion-related gold deposit, Tombstone gold belt, Yukon, Canada[J]. Econ. Geol., 101(3): 523-553.

Mao J W, Wang Y T, Lehmann B, Yu J, Du A D, Mei Y X, Li Y F, Zang W S, Stein H J and Zhou T F. Molybdenite Re-Os and albite $^{40}Ar/^{39}Ar$dating of Cu-Au-Mo and magnetite porphyry systems in the Changjiang valley and metallogenic implications[J]. Ore Geology Reviews, 29: 307-324.

Mcmanus A and Wallace M W. 1992. Age of mississippivalley type sulfides determined using cathodoluminesence cement stratigraphy, Lennard shelf, Canning basin, western Australia[J]. Econ. Geol., 87(1): 189-193.

Meinert L D. 1997. Application of skarn deposit zonation models to mineral exploration[J]. Exploration and Mining Geology, 6: 185-208.

Meinert L D, Dipple G M and Nicolescu S. 2005. World skarn deposits[J]. Economic Geology 100th Anniversary Volume. 299-336.

Müller A, Herrington R, Armstrong R, Seltman R, Kirwin D J, Stenina N G and Kronz A. 2010. Trace elements and cathodoluminescence of quartz in stockwork veins of Mongolian porphyry-style deposits[J]. Mineralium Deposita, 45(7): 707-727.

Nakano T, Takahara H and Norimasa N. 1989. Intracrystalline distribution of major elements in zoned garnet from skarn in the Chichibu mine, Central Japan: Illustration by color-coded maps[J]. Canadian Mineralogist, 27: 499-507.

Ni P, Wang X D, Wang G G, Huang J B, Pan J Y and Wang T G. 2015. An infrared microthermometric study of fluid inclusions in coexisting quartz and wolframite from Late Mesozoic tungsten deposits in the Gannan metallogenic belt, South China[J]. Ore Geology Reviews, 65: 1062-1077.

Nie L Q, Zhou T F, Fan Y, Zhang Q M, Zhang M and Wang L H. 2016a. LA-ICPMS U-Pb zircon age and molybdenite Re-Os dating of Donggushan, the first tungsten deposit found in the Luzong orefield, Middle-Lower Yangtze River Valley metallogenic belt[J]. Acta Petrologica Sinica, 32(2): 303-318(in Chinese with English abstract).

Nie L Q, Zhou T F, Fan Y, Zhang Q M, Zhang M, Wang L H and Ge J. 2016b. First discovery of a tungsten deposit in North of Luzong-orefield along Middle-Lower Yangtze River valley metallogenic belt[J]. Mineral Deposits, 35(5): 999-1010(in Chinese with English abstract).

Nie L Q, Zhou T, Fan Y, Cook D and White N. 2017. Geology, geochemistry and genesis of the Makou magnetite-apatite deposit in the Luzong volcanic basin, Middle-Lower Yangtze River Valley Metallogenic Belt, eastern China[J]. Ore Geology Reviews, 91: 264-277.

Nie L Q, Zhou T F, Wang F Y, Li X X and Wei O X. 2018. Scheelite trace element compositions from the Dongyuan deposit: Implications for tungsten mineralization[J]. Mineral Deposits, 37(6): 1237-1246(in Chinese with English abstract).

Ningwu Project Group. 1978. The porphyrite iron deposit in Ningwu area[J]. Beijing: Geological Publishing House. 1-320(in Chinese).

No. 1 Geological Party of Hubei Geological Bureau. 2018. Geological survey report of Fujiashan-Longjiaoshan deposit, Daye City, Hubei Province[R].

O'reilly C, Gallagher V and Feely M. 1997. Fluid inclusion study of the Ballinglen W-Sn-sulphide mineralization, SE Ireland[J]. Mineralium Deposita, 32(6): 569-580.

Orhan A. 2017. Evolution of the Mo-rich scheelite skarn mineralization at Kozbudaklar, western Anatolia, Turkey: Evidence from mineral chemistry and fluid inclusions[J]. Ore Geology Reviews, 80: 141-165.

Pan J Y, Ni P and Wang R C. 2019. Comparison of fluid processes in coexisting wolframite and quartz from a giant vein-type tungsten deposit, South China: Insights from detailed petrography and LA-ICP-MS analysis of fluid inclusions[J]. American Mineralogist, 104(8): 1092-1116.

Park C, Song Y, Kang I M, Sim J and Park C S. 2017. Metasomatic changes during periodic fluid flux recorded in grandite garnet from the Weondong W-skarn deposit, South Korea[J]. Chemical Geology, 451: 135-153.

Peng N J, Jiang S Y, Xiong S F and Pi D H. 2018. Fluid evolution and ore genesis of the Dalingshang deposit, Dahutang W-Cu ore field, northern Jiangxi Province, South China[J]. Mineralium Deposita, 53: 1079-1094.

Poulin R S, Mcdonald A M and Kontak D J. 2016. Then relationship between cathodoluminescence and the chemical chemical composition of scheelite from geologically diverse ore-deposit environments[J]. The Canadian Mineralogist, 54: 1147-1173.

Poulin R S, Kontak D J and McdonaldA M. 2018. Assessing scheelite as an ore-deposit discriminator using its trace-element and REE chemistry[J]. The Canadian Mineralogist, 56: 265-302.

Putnis. 2009. Mineral replacement reactions[J]. Reviews in Mineralogy and Geochemistry, 70: 87-124.

Qi H S, Yang X Y, Lu S M, Tang C, Cao Y J, Zhao L L, Deng J H, Sun C, Zhao Z and Lee I. 2020. Ore genesis and fluid evolution of the Qiaomaishan Cu-W deposit, in the Middle-Lower Yangtze River Metallogenic Belt: Evidence from in situ analyses of apatite and scheelite-ScienceDirect[J]. Ore Geology Reviews, 127, 103864

Raimbault L, Baumer A, Dubru M, Benkerrou C, Crose V and Zahm A. 1993. REE fractionation between scheelite and apatite in hydrothermal conditions[J]. American Mineralogist, 78(11): 1275-1285.

Redmond P B, Einaudi M T, Inan E E, Landtwing M R and Heinrich C A. 2004. Copper deposition by fluid cooling in intrusion-centered systems: New insights from the Bingham porphyry ore deposit, Utah[J]. Geology, 32(3): 217-220.

Reich M, Deditius A, Chryssoulis S, Li J W, Ma C Q, Parada M A, Barra F and Mittermayr F. 2013. Pyrite as a record of hydrothermal fluid evolution in a porphyry copper system: A SIMS/EMPA trace element study[J]. Geochimicaet Cosmochimica Acta, 104(1): 42-62.

Rempel K U, Williams-Jones A E and MigdisovAA. 2009. The partitioning of molybdenum (Ⅵ) between aqueous liquid and vapour at temperatures up to 370°C[J]. Geochimicaet Cosmochimica Acta, 73(11): 3381-3392.

Roberts S, Palmer M R and Waller L. 2006. Sm-Nd and REE characteristics of tourmaline and scheelite from the Bjorkdalgold deposit, northern Sweden: Evidence of an intrusion-related gold deposit[J]? Econ. Geol., 101(7): 1415-1425.

Rusk B G and Reed M H. 2002. Scanning electron microscope-cathodoluminescence analysis of quartz reveals complex growth histories in veins from the Butte porphyry copper deposit, Montana [J]. Geology, 30: 727-730.

Rusk B G, Lowers H A and Reed M H. 2008. Trace elements in hydrothermal quartz: Relationships to cathodoluminescent textures and insights into vein formation[J]. Geology, 36(7): 547-550.

Sciuba M, Beaudoin G and Grzela D. 2020. Trace element composition of scheelite in orogenic gold deposits[J]. Mineralium Deposita, 55 (12): 913-937

Shannon R D. 1976. Revised effective ionic radii and systematic studies of interatomic distances in halides and chalcogenides[J]. Acta Crystallographica Section A,32: 751-767.

Shu Q A, Chen P L and Cheng J R. 1992. Geology of iron-copper deposits in eastern Hubei Province, China[J]. Beijing: Metallurgic Industry Press. 1-532 (in Chinese with English abstract).

Shu Q H, Chang Z S, Hammerli J, Lai Y and Huizenga J M. 2017. Composition and evolution of fluids forming the Baiyinnuo' er Zn-Pb skarn deposit, northeastern China: Insights from laser ablation ICP-MS study of fluid inclusions[J]. Econ. Geol., 112(6): 1441-1460.

Singoyi B and Zaw K. 2001. A petrological and fluid inclusion study of magnetite-scheelite skarn mineralization at Kara, northwestern Tasmania: Implications for ore genesis[J]. Chemical Geology, 173 (1): 239-253.

Smith M, Henderson P, Jeffries T, Long J and Williams C. 2004. The rare earth elements and uranium in garnets from the Beinn an Dubhaich Aureole, Skye, Scotland, UK: Constraints on processes in a dynamic hydrothermal system[J]. Journal of Petrology, 45(3): 457-484.

Soloviev S G, Kryazhev S G and Dvurechenskaya S S. 2017. Geology, mineralization, stable isotope, and fluid inclusion characteristics of the Vostok-2 reduced W-Cu skarn and Au-W-Bi-As stockwork deposit, Sikhote-Alin, Russia[J]. Ore Geology Reviews, 86: 338-365.

Song G X, Qin K Z and Li G M. 2010. Study on the fluid inclusions and S-H-O isotopic composition of skarn-porphyry-type W-Mo deposits in Chizhou area in the Middle-Lower Yangtze Valley[J]. Acta Petrologica Sinica, 26(9): 2768-2782(in Chinese with English abstract).

Song G X, Qin K Z, Li G M, Evans N J and Chen L. 2014. Scheelite elemental and isotopic signatures: Implications for the genesis of skarn-type W-Mo deposits in the Chizhou area, Anhui Province, eastern China[J]. American Mineralogist, 99(2-3): 303-317.

Su S Q, Qin K Z, Li G M, Large R R, Olin P and Evans N J. 2021. Constraints on scheelite genesis at the Dabaoshan strata bound polymetallic deposit, South China[J]. American Mineralogist, 106 (9): 1503-1519.

Sun Y, Ma C Q and Liu Y Y. 2013. The Latest Yanshanian magmatic and metallogenic events in the Middle-Lower Yangtze River Belt: Evidence from the Ningzhen region[J]. Chinese Science Bulletin,

http://www.kcdz.ac.cn

58(34): 668-678(in Chinese with English abstract).

Sun K K and Chen B. 2017. Trace elements and Sr-Nd isotopes of scheelite: Implications for the W-Cu-Mo polymetallic mineralization of the Shimensi deposit, South China[J]. American Mineralogist, 102(5): 1114-1128.

Sverjensky D M. 1984. Europium redox equilibria in aqueous solution[J]. Earth Planet. Science Letter, 67: 70-78.

Uspensky E, Brugger J and Graeser S. 1998. REE geochemistry systematics of scheelite from the Alps using luminescence spectroscopy: From global regularities to local control[J]. Swiss Journal of Geosciences Supplement, 78(1): 31-54.

Wang F Y, Ge C, Ning S Y, Nie L Q, Zhong G X and White N. 2017. A new approach to LA-ICP-MS mapping and application in geology[J]. Atca Petrologica Sinica, 33(11): 3422-3436(in Chinese with English abstract).

Wang G G, Ni P and Pan J Y. 2020. Fluid characteristics of granite-related ore forming system[J]. Bulletin of Mineralogy, Petrology and Geochemistry, 39(3): 463-471+441(in Chinese with English abstract).

Wang M, Shang X, Zhang F, Wei K and Wang W. 2019. In-situ major and trace element chemistry of melanite from Tieshan Fe-Cu skarn deposit, Hubei Province, eastern China: Implications for hydrothermal fluid evolution[J]. Ore Geology Review, 111: 102996.

Wang S W, Zhou T F, Yuan F, Fan Y, Cao X S and Wang B. 2012. Re-Os and $^{40}Ar/^{39}Ar$ dating of the Shujiadian copper deposit in Tongling, China: Implicationg for regional metallogenesis[J]. Acta PetrologicaSinica, 28(10): 3170-3180(in Chinese with English abstract).

Wei W F, Hu R Z, Bi X W, Peng J T, Su W C, Song S Q and Shi S H. 2012. Infrared microthermometric and stable isotopic study of fluid inclusions in wolframite at the Xihuashan tungsten deposit, Jiangxi Province, China[J]. Mineralium Deposita, 47(6): 589-605.

Wood S A and Samson I M. 2000. The hydrothermal geochemistry of tungsten in granitoid environments: I. Relative solubilities of ferberite and scheelite as a function of *T*, *P*, pH, and mNaCl[J]. Econ. Geol., 95(1): 143-182.

Wu S, Mao J, Ireland T R, Zheng Z, Yao F J, Yang Y P and Sun W D. 2019. Comparative geochemical study of scheelite from the Shizhuyuan and Xianglushan tungsten skarn deposits, South China: Implications for scheelite mineralization[J]. Ore Geology Reviews, 109: 448-464.

Wu S, Sun W and Wang X. 2019. A new model for porphyry W mineralization in a world-class tungsten metallogenic belt[J]. Ore Geology Reviews, 107: 501-512.

Xiao Q, Zhou T F, Hollings P, Wang S W and Yuan F. 2021. The role of porphyry-related skarns in the Chating porphyry copper and gold deposit, eastern China[J]. Ore Geology Reviews, 133(11-12): 104096.

Xiao X, Zhou T F, White N C, Zhang L J, Fan Y, Wang F Y and Chen X F. 2018. The formation and trace elements of garnet in the skarn zone from the Xinqiao Cu-S-Fe-Au deposit, Tongling ore district, Anhui Province, eastern China[J]. Lithos, 302-303: 467-479.

Xie G Q, Mao J W, Li R L, Qü W J, Pirajno F and Du A D. 2007. Re-Os molybdenite and Ar-Ar phlogopite dating of Cu-Fe-Au-Mo (W) deposits in southeastern Hubei, China[J]. Mineralogy and Petrology, 90(3-4): 249-270.

Xie G Q, Li R L, Jiang G H, Zhao C S and Hou K J. 2008. Geochemistry and petrogenesis of Late Mesozoic granitoids in southeastern Hubei Province and constrains on the timing of lithospheric thinning, Middle-Lower Reaches of the Yangtze River, eastern China[J]. Acta Petrologica Sinica, 24(8): 1703-1714 (in Chinese with English abstract).

Xie G Q, Zhu Q Q, Yao L, Wang J and Li W. 2013. Discussion on regional metal mineral deposit model of Late Mesozoic Cu-Fe-Au polymetallic deposits in the southeast Hubei Province[J]. Bulletin of Mineralogy, Petrology and Geochemistry, 32(4): 418-426(in Chinese with English abstract).

Xie G W, Mao J M, Zhu Q Q, Yao L, Li Y and Li W. 2015. Geochemical constraints on Cu-Fe and Fe skarn deposits in the Edong district, Middle-Lower Yangtze River Metallogenic Belt, China[J]. Ore Geology Reviews, 64: 425-444.

Xiong Y Q, Shao Y J, Zhou H D, Wu Q H, Liu J P, Wei H T, Zhao R C and Cao JY. 2017. Ore-forming mechanism of quartz-vein-type W-Sn deposits of the Xitian district in SE China: Implications from the trace element analysis of wolframite and investigation of fluid inclusions[J]. Ore Geology Reviews, 83: 152-173.

Xu X C, Fan Z L, He J, Liu X, Liu X Y, Xie Q Q, Lu S M and Lou J W. 2014. Metallogenic model for the copper-gold-polymetallic deposits in Shizishan ore-field, Tongling, Anhui Province[J]. Acta Petrologica Sinica, 30(4): 1054-1074(in Chinese with English abstract).

Yan D R, Deng X D, Hu H and Li J W. 2012. U-Pb age and Petrogenesis of the Ruanjiawan granodiorite pluton and Xiniushan granodiorite porphyry, southeast Hubei Province: Implication for Cu-Mo mineralization[J]. Acta Petrologica Sinica, 28(10): 3337-3388(in Chinese with English abstract).

Yardley B, Rochelle C, Barnicoat A and Lloyd G. 1991. Oscillatory zoning in metamorphic minerals: An indicator of infiltration metasomatism[J]. Mineral Magzaine, 55(380): 357-365.

Zajacz Z, Halter W E, Pettke T and Guillong M. 2008. Determination of fluid/melt partition coefficients by LA-ICP-MS analysis of coexisting fluid and silicate melt inclusions: Controls on element partitioning[J]. Geochimica et Cosmochimica Acta, 72(8): 2169-2197.

Zhai D G, Liu J J, Zhang H Y, Wang J P, Su L, Yang X A and Wu S H. 2014. Origin of oscillatory zoned garnets from the Xieertala Fe-Zn skarn deposit, northern China: In situ LA-ICP-MS evidence[J]. Lithos, 190: 279-291.

Zhai Y S, Yao S Z and Lin X D. 1992. Copper and iron deposits in Lower Yangtze River[M]. Beijing: Geological Publishing House. 1-145(in Chinese).

http://www.kcdz.ac.cn/

Zhang L J, Zhou T F, Fan Y, Yuan F, Qian B and Ma L. 2011. A LA-ICP-MS study of apatite from the Taocun magnetite-apatite deposit, Ningwu Basin[J]. Acta Geologica Sinica, 85(5): 834-848(in Chinese with English abstract).

Zhang Q, Zhang R Q, Gao J F, Lu J J and Wu J W. 2018. In-situ LA-ICP-MS trace elemental analyses of scheelite and wolframite: Constraints on the genesis of veinlet-disseminated and vein-type tungsten deposits, South China[J]. Ore Geology Reviews, 99: 166-179.

Zhang S, Zhou T F, Zhang Z Z, Wu M A, Wang J and Lü Q T. 2021. In-situ hydrothermal zircon U-Pb and phlogopite ^{40}Ar-^{39}Ar geochronology of uranium mineralisation in Luzong ore district scientific drilling (LTZK01), Anhui Province, SE China: Constraints on the mineralisation process[J]. Ore Geology Reviews, 134: 104133.

Zhang W. 2017. Study of the characteristics of trace elements of chlorite and epidote in Luohe iron deposit, Anhui (Master Thesis)[D]. Supervisor: Fan Y. Hefei: Hefei University of Technology. 1-101 (Chinese with English abstract).

Zhao W W, Zhou M F, Williams-Jones A E and Zhao Z. 2018. Constraints on the uptake of REE by scheelite in the Baoshan tungsten skarn deposit, South China[J]. Chemical Geology, 477: 123-136.

Zhang Y, Shao Y J, Wu C D and Chen H Y. 2017. LA-ICP-MS trace element geochemistry of garnets: Constraints on hydrothermal fluid evolution and genesis of the Xinqiao Cu-S-Fe-Au deposit, eastern China[J]. Ore Geology Review, 86: 426-439.

Zhang Y, Ma D S and Gao J F. 2020. Origin and evolution of ore-forming fluids in a tungsten mineralization system, Middle Jiangnan orogenic belt, South China: Constraints from in-situ LA-ICP-MS analyses of scheelite-sciencedirect[J]. Ore Geology Reviews, 127: 103806.

Zhang Z Z, Wu M A, Du J G, Zhang S, Zhang Q M and Lu S M. 2018. Geochronology and geochemistry of the tungsten deposit-related granites in the Luzongore field: Petrogenesis and insights for Late Cretaceous metallogeny in the Middle and Lower Reaches of Yangtze River Metallogenic Belt[J]. Acta Petrologica Sinica, 34 (1): 217-240(in Chinese with English abstract).

Zhou T F, Fan Y, Yuan F, Song C Z, Zhang L J, Qian C C, Lu S M and David R C. 2010. Tempora-spatial framework of magmatic intrusions in Luzong volcanic basin in East China and their constrain to mineralization[J]. Acta Petrologica Sinica, 26(9): 2694-2714(in Chinese with English abstract).

Zhou T F, Fan Y, Yuan F and Zhong G X. 2012. Progress of geological study in the Middle-Lower Yangtze River Valley Metallogenic Belt[J]. Acta Petrologica Sinica, 28(10): 3051-3066(in Chinese with English abstract).

Zhou T F, Fan Y, Wang S W and White N. 2017. Metallogenic regularity and metallogenic model of the Middle-Lower Yangtze River Valley Metallogenic Belt[J]. Acta Petrologica Sinica, 33(11): 3353-3372(in Chinese with English abstract).

Zhou T F, Nie L Q, Fan Y, Wang F Y and Zhang Q M. 2019. Tungsten deposits in the Middle-Lower Yangtze Metallogenic Belt, China[J]. Acta Petrologica Sinica, 35(12): 3592-3608(in Chinese with English abstract).

Zhu Q Q, Xie G Q, Li W, Zhang F, Wang J, Zhang P and Yu B F. 2014. In situ analysis of garnets from the Jingshandian iron skarn deposit, Hubei Province, and its geological implications[J]. Geology in China, 41(6): 1944-1963(in Chinese with English abstract).

附中文参考文献

常印佛,刘湘培,吴言昌. 1991. 长江中下游铁铜成矿带[M]. 北京:地质出版社. 1-379.

陈雪锋,周涛发,张达玉,熊珍银,吕启良,袁峰,任志,范羽. 2017. 皖南池州桂林郑钼矿床成矿岩体的年代学和地球化学特征及其地质意义[J]. 岩石学报,33(10):3200-3216.

丁丽雪,黄圭成,夏金龙. 2014. 鄂东南地区龙角山-付家山斑岩体成因及其对成矿作用的指示[J]. 地质学报,88(8):1513-1527.

丁宁. 2012. 安徽省钨矿成矿规律(硕士论文)[D]. 导师:周涛发,杜建国. 合肥:合肥工业大学.155 页.

范裕,周涛发,袁峰,张乐骏,钱兵,马良,谢杰,杨西飞. 2011. 宁芜盆地玢岩型铁矿床的成矿时代:金云母 ^{40}Ar-^{39}Ar 同位素年代学研究[J]. 地质学报,85(5):810-820.

纪云昊,谢桂青,朱乔乔,孙孝峰,李新昊. 2019. 含碳质地层对矽卡岩钨矿的影响——以鄂东付家山钨矿床为例[J]. 矿床地质,38(4):917-934.

湖北省第一地质大队. 2018. 湖北省大冶市付家山-龙角山矿床地质调查报告[R],

蒋少涌,赵葵东,姜海,苏慧敏,熊索菲,熊伊曲,徐耀明,章伟,朱律运. 2020. 中国钨锡矿床时空分布规律、地质特征与成矿机制研究进展[J]. 科学通报,65(33):3730-3745.

刘畅,赵正,陆丽娜,曾载淋,刘翠辉,许虹. 2018. 南岭东段岩前矽卡岩型钨矿成矿流体研究[J]. 地质学报,92(12):2485-2507.

刘善宝,王登红,陈毓川,许建祥,曾载林,应立娟,王成辉. 2007. 南岭东段赣南地区天门山花岗岩体及花岗斑岩脉的 SHRIMP 定年及其意义[J]. 地质学报,81:972-978.

鲁麟,梁婷,任文琴,赵正,刘善宝,陈郑辉. 2018. 赣南淘锡坑石英脉型钨矿床成矿机制探讨:来自流体包裹体的证据[J]. 矿床地质,37(6):1260-1280.

聂利青,周涛发,范裕,张千明,张明,汪龙虎. 2016a. 长江中下游成矿带庐枞矿集区首例钨矿床成岩成矿时代及其意义[J]. 岩石学报,32(2):303-318.

聂利青,周涛发,范裕,张千明,张明,汪龙虎,葛靖. 2016b. 长江中下游成矿带庐枞矿集区新发现钨多金属矿床[J]. 矿床地质,35(5):999-1010.

聂利青,周涛发,汪方跃,张达玉,陈雪锋,肖庆玲,李旋旋,位欧详. 2018. 安徽省东源斑岩型钨矿床白钨矿原位微量元素特征及其指示意义[J]. 矿床地质, 37(6):1237-1246.

宁芜玢岩铁矿编写组. 1978. 宁芜玢岩铁矿[M]. 北京:地质出版社. 1-320.

舒全安,陈培良,程建荣. 1992. 鄂东铁铜矿产地质[M]. 北京:冶金工业出版社. 1-532.

http://www.kcdz.ac.cn

宋国学，秦克章，李光明. 2010. 长江中下游池州地区矽卡岩-斑岩型W-Mo矿床流体包裹体与H、O、S同位素研究[J]. 岩石学报，26(9)：2768-2782.

孙洋，马昌前，刘园园. 2014. 长江中下游燕山期最新的成岩成矿事件：来自宁镇地区的证据[J]. 科学通报，59(8)：668-678.

汪方跃，葛粲，宁思远，聂利青，钟国雄，White N C. 2017. 一个新的矿物面扫描分析方法开发和地质学应用[J]. 岩石学报，33(11)：3422-3436.

王国光，倪培，潘君屹. 2020. 花岗质岩石相关成矿系统的流体作用[J]. 矿物岩石地球化学通报，39(3)：463-471+441.

王世伟，周涛发，袁峰，范裕，曹晓生，王彪. 2012. 铜陵舒家店斑岩铜矿成矿年代学研究及其成矿意义[J]. 岩石学报，28(10)：3170-3180.

谢桂青，李瑞玲，蒋国豪，赵财胜，侯可军. 2008. 鄂东南地区晚中生代侵入岩的地球化学和成因及对岩石圈减薄时限的制约[J]. 岩石学报，24：1703-1714.

谢桂青，朱乔乔，姚磊，王建，李伟. 2013. 鄂东南地区晚中生代铜铁金多金属矿的区域成矿模型探讨[J]. 矿物岩石地球化学通报，32(4)：418-426.

徐晓春，范子良，何俊，刘雪，刘晓燕，谢巧勤，陆三明，楼金伟. 2014. 安徽铜陵狮子山矿田铜金多金属矿床的成矿模式[J]. 岩石学报，30(4)：1054-1074.

颜代蓉，邓晓东，胡浩，李建威. 2012. 鄂东南地区阮家湾和犀牛山花岗闪长岩的时代、成因及成矿和找矿意义[J]. 岩石学报，28(10)：3373-3388.

翟裕生，姚书振，林新多，周珣若，万天丰，金福全，周永桂. 1992. 长江中下游地区铁铜(金)成矿规律[M]. 北京：地质出版社. 1-235.

张乐骏，周涛发，范裕，袁峰，钱兵，马良. 2011. 宁芜盆地陶村铁矿床磷灰石的LA-ICP-MS研究[J]. 地质学报，85(5)：834-848.

张维. 2017. 安徽罗河铁矿床绿泥石和绿帘石微量元素特征研究(硕士论文)[D]. 导师：范裕. 合肥：合肥工业大学. 101页.

张赞赞，吴明安，杜建国，张舒，张千明，陆三明. 2018. 庐枞矿集区与钨矿床有关的花岗岩的年代学及地球化学特征:岩石成因及其对长江中下游晚白垩世成矿的启示[J]. 岩石学报，34(1)：217-240.

钟国雄，周涛发，袁峰，蒋其胜，范裕，张达玉，黄建满. 2014. 安徽铜陵姚家岭大型锌金矿床中新发现白钨矿[J]. 地质学报，88(4)：620-629.

周涛发，张乐骏，袁峰，范裕，Cooke DR. 2010. 安徽铜陵新桥Cu-Au-S矿床黄铁矿微量元素LA-ICP-MS原位测定及其对矿床成因的制约[J]. 地学前缘，17(2)：306-319.

周涛发，范裕，袁峰，钟国雄. 2012. 长江中下游成矿带地质与矿产研究进展[J]. 岩石学报，28(10)：3051-3066.

周涛发，范裕，王世伟，Noel C W. 2017. 长江中下游成矿带成矿规律和成矿模式[J]. 岩石学报，33(11)：3353-3372.

周涛发，聂利青，王世伟，汪方跃，张千明. 2019. 长江中下游成矿带钨矿床[J]. 岩石学报，35(12)：3592-3608.

朱乔乔，谢桂青，李伟，张帆，王建，张平，于炳飞. 2014. 湖北金山店大型矽卡岩型铁矿石榴子石原位微区分析及其地质意义[J]. 中国地质，41(6)：1944-1963.

http://www.kcdz.ac.cn